THE GROWTH PRESSURE OF FIBROUS SODIUM CHLORIDE

THESIS PREPARED IN PARTIAL FULFILLMENT OF THE
REQUIREMENTS FOR THE DEGREE OF
MASTER OF SCIENCE IN GEOLOGY
AT THE
NEW MEXICO INSTITUTE OF MINING AND TECHNOLOGY

BY
JACQUES R. RENAULT

TABLE OF CONTENTS

ILLUSTRATIONS

Tables

Figures

ABSTRACT

Direct measurement of the growth pressure of NaCl fibers shows that they can exert a force of 24.6 bars against a static load. The growth rate of the fibers is correlated with the applied load and a relationship is suggested for determining the growth pressure from the growth rates of loaded crystals. A tentative maximum growth pressure is calculated from the growth rates at varying loads and found to agree substantially with the measured growth pressure.

X-ray studies of the fibers reveal a [100] orientation of the fiber axes.

Salt growths from Zuni Salt Lake, New Mexico, were not found to occur as fibers such as those grown artificially for this investigation. The crystallization of halite was found to figure significantly in the disintegration of rocks at the margin of the lake.

INTRODUCTION

The ability of crystals to grow under an uniaxial stress has been considered by several authors, Becker and Day (1905, 1916), Taber (1916a, 1916b), Correns (1926, 1949), Schubnikov (1934), Cooke (1936), and Ramberg (1947, 1952). Becker and Day, Taber, Correns, and Schubnikov proved experimentally that an alum crystal growing in a supersaturated solution could lift a superimposed load. Correns (1926) developed an equation for the growth pressure of a crystal growing in a solution, and Ramberg (1947) developed a general equation for a crystal growing in any environment.

In 1952 Ramberg defined growth pressure (or force of crystallization) as ". . . the excess pressure which must be applied on the crystal in order that the crystal may be in chemical equilibrium with its surroundings, which are supersaturated to a given degree." The term "growth pressure" (Buckley, 1951) is used in this investigation in preference to "force of crystallization" as the latter may be confused with the ability of some minerals to form idioblastic grains when growing in a metamorphic environment.

Taber (1916b) and later Cooke (1936) studied the asbestos vein deposits of Thetford, Quebec; they postulated a growth pressure or force of crystallization to explain the cross-fiber habit of the asbestos.

To the author's knowledge, no attempts to measure the growth pressure of fibrous crystals in contact with solution only at their bases have been made. However, experiments involving the growth of loaded crystals completely immersed in a super-saturated solution have been conducted. The common occurrence in nature of cross-fiber veins of gypsum, epsom salt, alum, and asbestos prompted this investigation. Fibrous NaCl was chosen for study because of the ease with which the fibrous habit may be induced. However, natural cross-fiber halite veins have not been observed by the author, nor has mention of them been found in the literature.

The author wishes to express his appreciation to Dr. F. J. Kuellmer, who was thesis advisor for this investigation and whose guidance and interest in the problem were invaluable. The author also wishes to express his thanks to Dr. A. J. Budding, Dr. C. T. Smith, and Dr. M. S. Sun for many helpful suggestions and to the members of the New Mexico Bureau of Mines and Mineral Resources for many interesting and pertinent discussions. The author is indebted

to the Geology Department of the New Mexico Institute of Mining and Technology and to the New Mexico Geological Society for the financial aid necessary to pursue this investigation, and to the New Mexico Bureau of Mines and Mineral Resources for permission to use their X-ray equipment and laboratory facilities. Photographs for Figures 3-7 were taken by Mr. Chung-Hung Hu and the manuscript was typed by Joann Huenergardt and Nadine Richards.

APPARATUS

An apparatus (see figures 1 and 2) was constructed to detect and measure crystal growth. The apparatus was not designed to record the absolute amount of growth, but relative changes in the growth rate could be determined.

The sample mount is placed on a steel stand of welded 1/2" x 6" steel plates (see figure 1). The bottom member of the stand is fitted with three leveling screws and the top member with the vertical adjustment screw supporting the mirror assembly of the optical lever system. The light source and focusing lens are held in place by laboratory ring stands and clamps. The two mirror components were made by cementing first-surface mirrors onto one side of square aluminum box-sections which were drilled to fit a fixed horizontal axle. This axle is rigidly attached to the vertical adjustment screw. The fixed mirror component can be adjusted to any rotational position and is held in that position by a rubber band. The growth mirror component is free to rotate about the axle, and when it is placed so as to reflect a light beam to a screen, it has a tendency to rotate about the axle due to the off-center mass of the mirror. A short finger in contact with a wire attached to the alundum disc on top of the sample mount permits the growth mirror to rotate only when the alundum disc moves. As the salt fibers grow, the

alundum disc moves upward and the corresponding movement of the growth mirror deflects the beam of light. Alundum was chosen for its strength and porosity.

The alundum disc lies on the top of the sample mount and, via this disc, load is applied to the fibers by means of a load beam and load pan assembly. The beam has a centering screw to concentrate the load at any point desired on the alundum disc. The load is placed in the pan, which is suspended from the beam by steel wires. By this means the load can be concentrated at the center of the growth area so that growth will not be more favorable at one position on the ceramic than on another. It was found that if the load were not centered, fibers would tend to grow faster where the pressure was the least.

The G. E. light-source contains a plano convex condensing lens across the plane side of which a cross hair of 0.002 inch diameter copper wire is cemented. An image of the cross hair is focussed onto a vertical screen at a distance of 4.8 meters by means of a meniscus lens. The leverage of the optical system varies with the distance between the wire on the alundum disc and the axle of the mirror assembly, but for a single set of runs, the error in resetting the apparatus can be kept within 1.1 percent. A magnification of X 940 was obtained for most of the runs, but if fibers grew faster on one side than on another, additional leverage could raise the

magnification to around X 2000, depending upon the geometry of the system.

The mirror assembly can be adjusted to cast an essentially horizontal beam by means of the vertical adjustment screw. The fixed mirror determines if the apparatus has been disturbed between observations; the movable mirror reflects any growth occurring between observations. At each observation the positions of the images reflected from both mirrors is noted on the screen by drawing a line at the position of the cross-hair image.

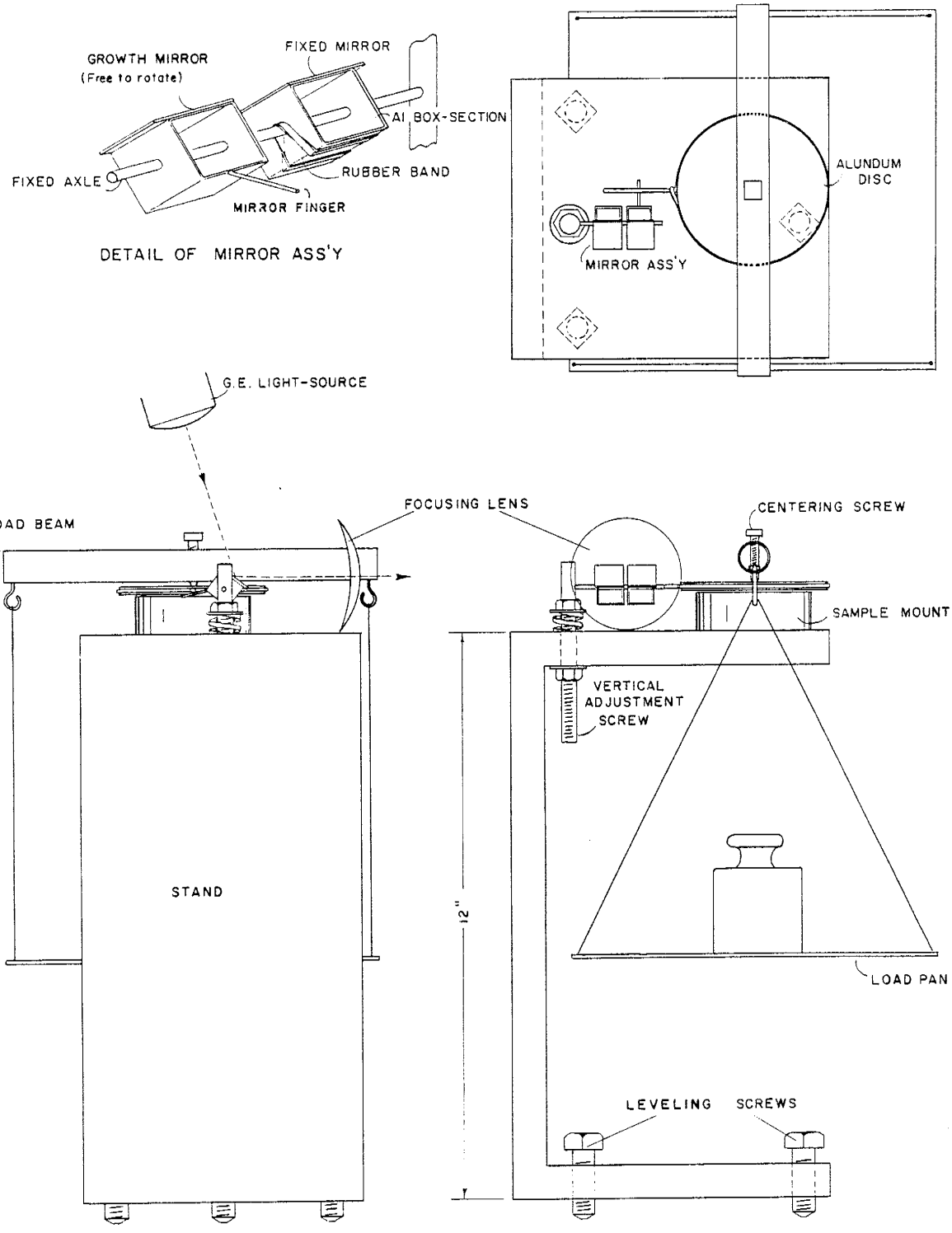

Fig. 1 SCHEMATIC DIAGRAM OF APPARATUS (not to scale)

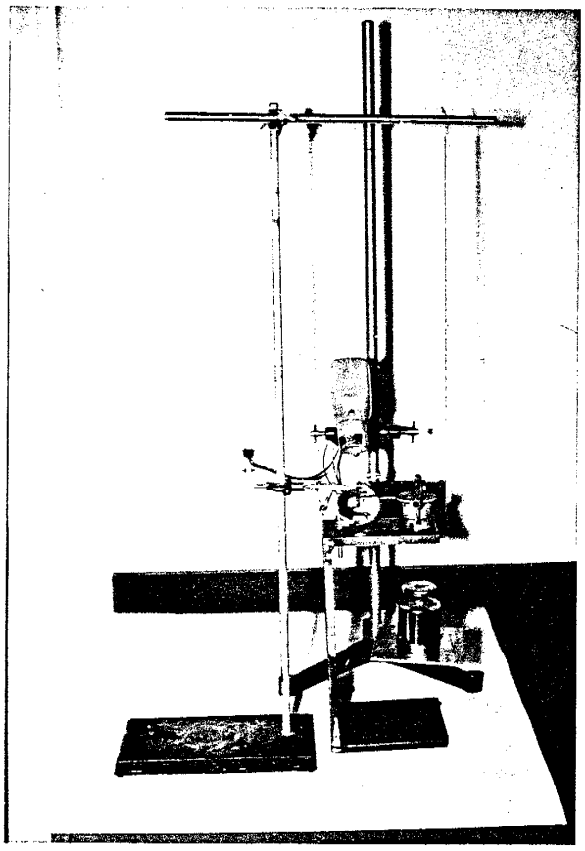

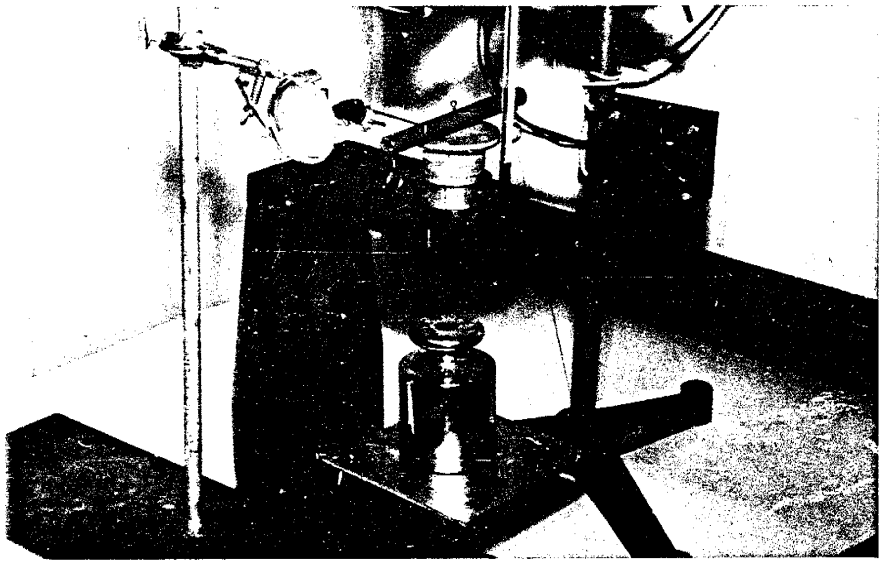

Figure 2. Two views of the apparatus for measuring the growth pressure of NaCl fibers.

PREPARATION OF ARTIFICIAL NaCl FIBERS

Synthesis

A standard NaCl-H_2O solution was prepared by disolving pharmaceutical grade NaCl in distilled water. The degree of saturation of the solution was determined by density measurements from data given in the 38th edition of the Handbook of Chemistry and Physics. At 20°C the solution was 19.6 percent undersaturated. A ceramic mount was then soaked in a portion of the standard solution for a period of 36 to 48 hours in a closed container. In order that air could escape freely from the pores of the ceramic, the mount was only partially immersed in the solution. When saturation of the mount with solution was essentially complete, as evidenced by dampness at the ceramic-air interface, the mount was removed from the solution and water allowed to evaporate from it. Crystallization is initiated with the appearance of a salt crust composed of spherical aggregates of randomly oriented grains (see figure 3) at the mount-air interface. After a period of a day to several days fibers appear, which elevate the crust above the mount surface. Termination of growth by complete evaporation was not observed, but in the case of mount ACB-3, salt crystallized continuously as fibers for over two months.

Figure 3. Spherical aggregates of NaCl (X 23) formed at the onset of crystallization

Construction of the mount

Fibrous NaCl will grow on a number of porous media such as clay (Schmidt, 1914), collodion membranes (Tauber and Kleiner, 1932), silica gel (Hinegardner, 1935), porcelain and brick (Gyulai, 1955), cellophane membranes (Amelynkx, 1958), and basalt scoria. Experiments showed that annealing cups manufactured by the Denver Fire Clay Co. served as a satisfactory medium for fibrous growth of NaCl. These cups are unglazed and have an effective porosity of about 19 percent. A no. 2 cup was used, which has the form of a truncated cone with its base the smaller diameter. The shape of the cup is not important for the growth of fibers; however, centering the load is facilitated if growth takes place on a circular surface.

According to Correns (1949), the growth pressure of a crystal growing in an aqueous solution of its ions depends, among other things, upon the degree of supersaturation of the solution. Thus, it is necessary that the fibers be permitted to grow only on the surface at which the load is applied; otherwise, unloaded crystals would grow at the expense of loaded crystals due to greater effective supersaturation in the vicinity of the former. Of course, this is true only for crystals whose solubility increases as the load upon them increases. In order that growth be restricted

to the area of loading and to a direction perpendicular to the plane of loading, Cerro-Bend* is molded around the ceramic.

The mount is then faced on a lathe in order to obtain plane parallel surfaces and to expose an annular surface of ceramic (see figures 4 and 5).

---

*Cerro-Bend is a eutectic alloy of 50.0% Bi, 26.7% Pb, 13.3% Sn, and 10.0% Cd. It melts at 70.0°C and expands slightly upon cooling. This expansion effectively prevents growth from occurring anywhere except at the air-ceramic interface by sealing pores in contact with the metal.

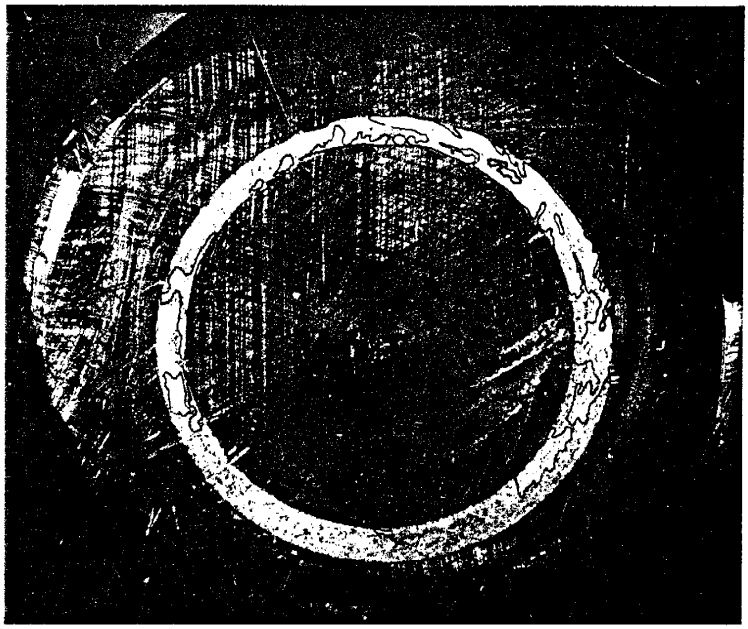

Figure 4. Top of ACB-3 (X 2.5) showing areas of crystal growth which are lighter in color and outlined in ink.

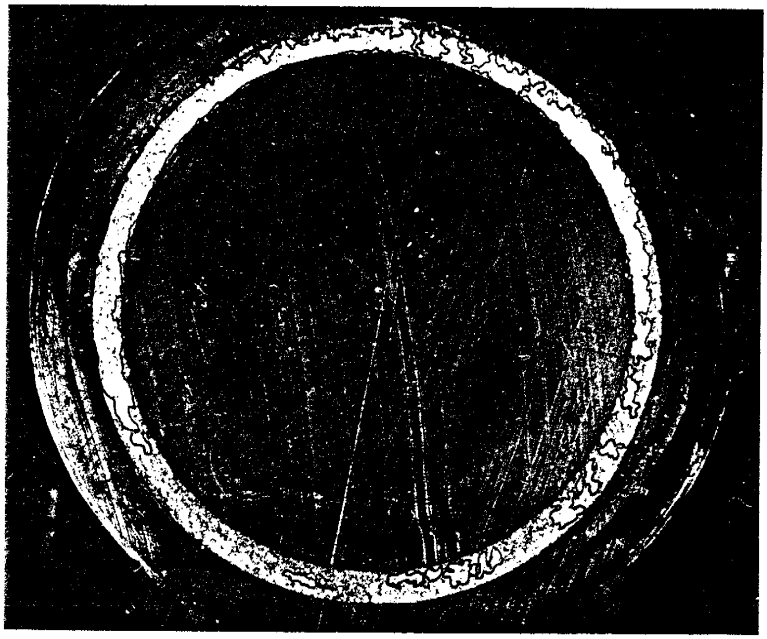

Figure 5. Bottom of ACB-3 (X 2.5) showing areas of crystal growth as in figure 4.

DESCRIPTION OF ARTIFICIAL NaCl FIBERS

NaCl fibers grown during this investigation are of two types. The first is a "single" straight fiber grown during the first preliminary trials, and the second is an aggregate of fibers with some degree of curvature.

Single fibers

Single fibers were first grown on an annealing cup which had been saturated with a salt solution and stored in a metal container for nine days. After this period of time single fibers had developed which were up to two centimeters long and about one micron in smallest diameter. Fiber aggregates also were present. In some fibers the thickness decreased stepwise one to three times over the length of the fiber. It was not determined whether this represented multiplicity of fibers or a cleavage parallel to the fiber axis. This type of fibrous growth was not repeated in subsequent experiments although single fibers did form in the laboratory as natural growth on a basalt sample collected from Zuni Salt Lake (see page 50).

Fibers similar to those described above seem to have been grown by Gyulai (1954) _ paper translated by Dr. Kuellmer –

on a brine saturated ceramic medium in an atmosphere nearly in equilibrium with a saturated salt solution. Gyulai's apparatus established a slight concentration gradient in the atmosphere above the solution by means of a small hole at the top of the crystallization chamber through which air was free to pass.

Fiber aggregates

The second type of fiber is an aggregate which, when unrestricted in its growth, generally grows in curly forms (see figure 6), with cork-screw and re-curved forms common. Growth of the fibers under external load tends to restrict growth to a direction normal to the loading plane and encourages dense packing of the fibers (see figure 7). Loaded fibers usually show some curvature, but it is slight and observable only under the microscope. The fibrous habit is defined microscopically by fine striae, and megascopically by a silky sheen. Individual fibers can be resolved only with difficulty at 450 diameters and never with great certainty at that magnification. The size appears to vary somewhat, with the larger individuals measuring about one micron in thickness. The length of the fibers grown under load did not exceed one millimeter, although unloaded curly aggregates in excess of three millimeters were obtained.

Figure 6. Detail of ACB-3 (X 9). CF = curly fibrous aggregate, F = columnar fibrous aggregate, and S = spherical aggregate.

Figure 7. Columnar fibrous aggregates (X 23), from ACB-3. Fibers grew under a load of 10.5 Kg/cm^2.

Small fiber aggregates of the order of 0.1 mm in diameter usually show uniform transparency, although internal reflection renders them only imperfectly transparent. The aggregates are quite brittle, which makes handling for X-ray purposes difficult. This brittleness is contrary to the property of flexibility possessed by the single fibers grown by Gyulai (1954).

GROWTH PRESSURE OF FIBROUS NaCl

Introduction

The growth pressure of growing crystals was originally investigated by Becker and Day (1905), who found that an alum crystal growing in a supersaturated solution could support a load and still continue to grow. They suggested that the maximum load which can be lifted by a growing crystal is limited by the crystal's crushing strength. Both Becker and Day (1916) and Taber (1916a) showed that a requirement for growth under load is the absence of unstressed crystals in the same solution with the stressed ones. It was apparent to them that the degree of supersaturation of the solution determined the growth pressure for a given crystal.

Subsequently, Correns (1926, 1949) presented experimental data on the ability of alum crystals to lift loads and showed that the theoretical maximum pressure which a crystal can support and be in equilibrium with its solution is proportional to the concentration of the solution and given by the relation

$$P_m = \frac{1}{V} RT \ln (c/c_s) \qquad (1)$$

where V is the molal volume of the crystal, R is the gas constant, T is the absolute temperature, and c and c_s are the actual and saturated concentrations respectively.

The maximum growth pressure

The theoretical maximum pressure which a crystal can support without dissolving would be determined only by the natural logarithm of the ratio c/c_s, which mathematically has no upper limit. However, a practical maximum pressure is determined by the most highly supersaturated solution which can exist without the spontaneous formation of embryonic crystals (auto-nucleation). The highest supersaturation for NaCl found in the literature is given by Kern (1953) as 44.0 g NaCl/100g H_2O. According to Kern, at this concentration the [111] form develops on preexisting crystals possessing only (100) and/or (110) faces when the concentration is raised to the given value. From equation (1), the growth pressure at this concentration would be 189 Kg/cm^2 where the concentration at saturation is taken as 35.9 g NaCl/100 g H_2O. This corresponds to a pressure of 2,690 psi, which is of the same order of magnitude as compressive strengths of 1,080 psi and 5,000 psi given by Wuerker (1956) for two different samples of rock salt. The figures also seem to corroborate the hypothesis of Becker and Day (1916) regarding

crushing strength as a maximum load limit on growing crystals. However, the persistence of the {100} form to the exclusion of all others under normal conditions indicates that concentrations as high as that measured by Kern (1953) rarely if ever exist in nature.

Correns (1949) measured the growth pressure of crystals completely immersed in solution and found that at high degrees of supersaturation, the experimental maximum growth pressure was less than the theoretical pressure and that the difference increased with the supersaturation. As noted before, it is important that no unstressed crystals be present in the solution with the stressed one. With regard to the difference between Correns' calculated and observed growth pressures, one can draw an analogy between the existence of unstressed faces and unstressed crystals in the solution. In fact, Correns found that the experimental maximum pressure of a stressed (111) face of alum was less than that of a stressed (110) face. Correns expressed the discrepancy in terms of surface energy as well as the presence of unstressed faces.

The method of measuring growth pressure used during this investigation differs from that of Becker and Day, Correns, and Schubnikov in that because fibrous crystals are used, essentially only one crystal face is in contact with the solution. Thus

the difficulty of having more than one kind of face in the solution is avoided insofar as the fibers have a preferred orientation and the base of the fiber is a single face. Of course, it is necessary that all of the fibers be equally stressed, and this is accomplished in the apparatus by restricting fibrous growth to a direction perpendicular to the plane of loading so that sooner or later a growing crystal will come in contact with the load.

Experimental procedure

After the mount has been soaked in a nearly saturated solution, it is removed, dried, and salt crust allowed to form on the ceramic surface by evaporation. If the evaporation rate is too great, or the grain size of the medium is too large, fibers will not grow. Fibers were never observed to grow without the prior formation of a salt crust. Attempts to grow fibers on sandstone and siltstone were unsuccessful as were attempts to grow salt fibers under load without first allowing a crust to form.

After the first fibers have appeared, the alundum disc (see figure 1) is placed over the growth area, and the wire attached to the disc is placed over the finger of the growth mirror component of the optical lever system. The load is then centered at the centroid of the growth area and the apparatus leveled in order to make the

surface of the ceramic normal to the direction of loading. The front lens of the optical lever system is then focussed to project a sharp image of the cross-hair onto the screen.

The position of the images reflected by the fixed mirror and the growth mirror are marked on the screen, and changes of the image position with time are similarly recorded. Both temperature and time are recorded at each observation as well as the displacement in millimeters of the growth mirror image. Any change in the position of the image reflected by the fixed mirror is taken as representing a disturbance of the apparatus and a corresponding displacement is added or subtracted, as the case may be, from that shown by the growth mirror. The growth data are tabulated, and a temperature correction due to the thermal expansion of the vertical adjustment screw is applied. The expansion of this screw has the effect of decreasing the apparent displacement of the image due to growth. All data were reduced to growth at $70^{\circ}F$ which is less than any temperature observed. The vertical adjustment screw is made of cold rolled brass, and its linear coefficient of expansion is taken as $20 \times 10^{-6}/C^{\circ}$.

The pressure applied to the fibers is calculated from the known load and the measured area of crystal growth. Several methods of area measurement were tried which consisted of the

use of a micrometer ocular in a microscope, camera lucida and planimeter, photographs and planimeter, and finally a method of sector measurement which was the most satisfactory. It ultimately became apparent that a small patch of fibers visible at the ceramic surface does not necessarily represent the total area under load in its immediate vicinity, for as growth was allowed to proceed, the surface of the ceramic bulged up in places and cracks developed which revealed fibers growing just beneath the surface (see figure 8). It was thus necessary to take the whole width of the ceramic surface as one dimension of the growth area, and as the growth area was annular, angular sector measurements of the growth area were taken, summed, and the ratio of the total growth sector to 360° taken as equal to the ratio of the total growth area to the total annular area of the ceramic surface. The precision of the measurement is good to $\pm$ 5 percent. The total area measured is undoubtedly too high due to spaces between fibers, but the absolute error was not evaluated. It probably lies between 10 and 20 percent.

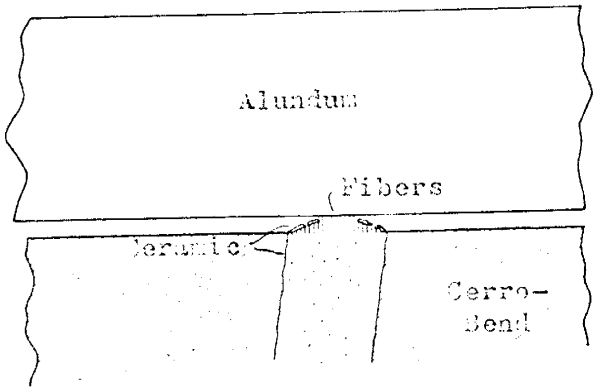

Figure 8. Cross-section through mount showing fibrous crystal growth bulging ceramic surface upward. Size exaggeration is about X 5.

Experimental results

During the first few runs with mount ACB-3 the load was augmented after suitable periods of growth without dismounting the apparatus. When the load had been augmented several times, the apparatus was dismounted and the area of growth measured. It was found that the ceramic surface of ACB-3 was too great, and a load sufficiently large to arrest growth could not be placed on the apparatus. ACB-8 was prepared from an annealing cup which was ground to a thinner wall size. A maximum pressure was achieved with this mount which arrested growth.

Curves of accumulated growth versus time for mount ACB-3 (see figures 10-13) show a systematic decrease in growth rate with increase in load pressure. This is to be expected, as an increase in the load applied to a growing crystal should increase its solubility and thus decrease the effective supersaturation of the solution. One would expect the growth rate to decrease as the supersaturation decreases, and in fact, Chrétien, Heubel, and Trimolé (1954) showed empirically that the growth rate of NaCl crystals is directly proportional to the square of the percent supersaturation.

A summary of experimentally obtained data is given in Table I together with a graph (figure 9) showing the relationship between growth rate and load. In the table P_n is the pressure under which the crystals grew during the various runs; r' and r'' are the initial and straight-line growth rates respectively (see figures 10-16). Stars indicate absence of data. In figure 9 the curve is drawn through the points representing straight-line growth rate versus pressure (P_n), because these measurements are the most reliable. The deviation of runs 1 and 3 of ACB-8 from the curve will be discussed in the next section.

The maximum observed pressure in equilibrium with the solution in the mount is 24.6 ± 1.0 bars. This pressure arrested

growth but did not cause dissolution. The probable error of $\pm$ 1.0 bar is based on a 5 percent error in the measurement of the growth area and a negligible error in the determination of the load.

It is seen on the curve of figure 9 that six points fit very well. As these points were determined from measurements taken on two different mounts, the curve suggests that a fairly uniform degree of supersaturation was maintained -- assuming, of course, that there is a regular relationship between growth rate and pressure. Solving for the concentration ratio in Correns' equation (page 13) gives a supersaturation of 2.7 percent. Such a concentration is not unreasonable and is probably attainable in nature.

Interpretation of results

Consideration of the shape of the growth rate curves of figures 10-16 is of great help in the interpretation of the data given above. Of particular interest is the concave-upward portion of the growth rate curves for runs 1, 2, 4, and 5 of ACB-3 and runs 1, 2, and perhaps 3 of ACB-8 in figures 10-14. Two assumptions are necessary to explain this behavior; namely, 1) that evaporation rate is relatively constant, and 2) that crystal nuclei of NaCl will form at relatively low degrees of supersaturation. Under these

Mount	Run	Load (Kg)	Duration (hr)	Growth Rate (mm/hr) x 10^3		P_n (Bars)	
				r'	r''	at r'	at r''
ACB-3	1	1.264	47.5	0.346	6.03	*	*
"	2	2.264	44.4	5.02-	5.02	*	*
"	3	4.264	29.2	3.04	3.04	*	*
"	4	8.081	19.9	1.16	1.89	*	10.5
"	5	15.201	928.1	0.274	0.775	19.7	16.1
ACB-8	1	1.264	39.2	0.638	2.70	*	4.13
"	2	2.264	25.0	0.425	2.83	7.40	7.40
"	3	4.264	24.8	2.57-	2.57	14.0	14.0
"	4	7.453	19.6	1.46	0.000	24.6	24.6
"	5	9.453	24.7	1.28	-0.053	31.2	31.2

TABLE I. Summary of Experimental Data

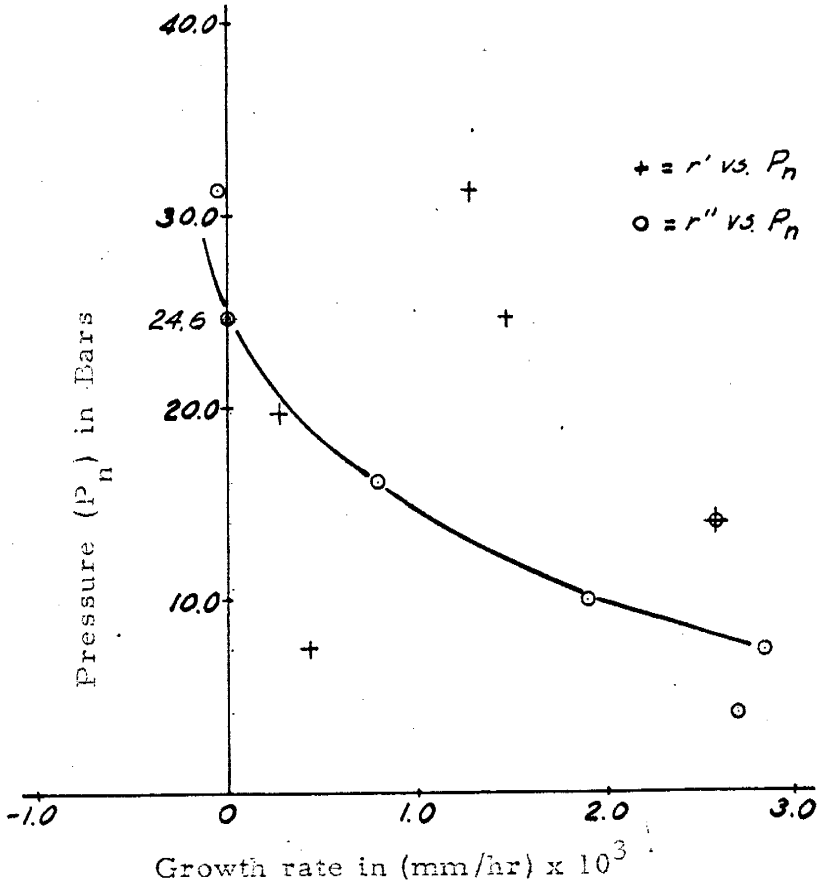

Figure 9. Graph of growth rate versus pressure

conditions, a relatively constant equilibrium growth rate will exist for stressed or unstressed crystals. If the load is increased and the evaporation rate remains constant, the growth rate will decrease and the supersaturation of the solution will increase until auto-nucleation occurs. At this point, the concentration will begin to decrease with the growth of new fibers. As soon as the new fibers begin to bear upon the load, the overall pressure per fiber will decrease, and the growth rate of the loaded crystals will increase to a value which is commensurate with the initial concentration of the solution and the increased load.

The slight decrease in growth rate after the linear portion of run 5 of ACB-3 in figure 13 probably is due to imperfect diffusion of ions in the solution. No departure from a linear growth rate is seen at the beginning of run 3 of ACB-3 (figure 12) and this is taken to mean that the increase in supersaturation due to augmentation of the load was not sufficient to cause auto-nucleation at that time. The slight convex-upward portion of the curve at the end of the run may indicate that auto-nucleation finally took place and that the presence of unstressed crystals caused the apparent growth rate to decrease. The convex-upward portion of the growth rate curve for run 1 of ACB-8, figure 14, is taken as representing a highly metastable condition of supersaturation during which nucleation did not begin

until the run was well under way. When the new crystals did begin to grow, the growth rate of the preexisting ones decreased until the new ones began to push on the load and diminish the overall pressure.

The pressure measurements for the early runs of ACB-8 are less reliable than the runs of ACB-3 and the later runs of ACB-8 because the growth area measured at the end of run 1 (ACB-8) was overestimated -- it was taken as the total area of the ceramic surface. The curve for run 2 (ACB-8) is concave upward because room existed for new crystals to grow. New fibers may have found space in which to grow during run 3 (ACB-8), but concavity is poorly defined here. The fact that run 3 deviates more from the curve in Figure 9 than runs 2, 4, and 5 (ACB-8) is anomalous and remains unexplained.

The convex-upward portions of the initial growth of runs 4 and 5 of ACB-8 in conjunction with the zero growth rate at the end of run 4 probably are due to augmentation of the load and represent increases in supersaturation and lack of space for new fibers to grow.

It might be expected that the occupation of the ceramic surface by new crystals would necessarily decrease the area of evaporation and thus the evaporation rate. Two factors tend to negate this effect; 1) the formation of the salt crust in the region where the fibers grow initially restricts effective evaporation to the margins of the ceramic surface, and 2) the existence of a salt "glaze" on areas where the

crust did not form prevents evaporation from these places. Toward the end of run 5 of ACB-3, the glazed portion of the ceramic surface was eventually pushed up and fractured by fibrous growth from beneath. This is interpreted as being due to approaching exhaustion and lowering of the solution in the capillary pores which resulted in the growth of new fibers below the ceramic surface.

The negative growth rates at the beginning of run 5 of ACB-8 are due to the appearance of crystals on the underside of the mount. This growth probably was caused by seeding from a highly supersaturated solution. The ceramic surface on the underside of the mount is larger in diameter than that on the top, and crystals growing on the side away from the mirror assembly caused an apparent negative growth rate. Their growth was sporadic as indicated by the return to a positive growth rate followed by another period of negative growth rate which was in turn followed by positive growth. The gap in the growth curve represents a lapse of time wherein a small amount of 19.6 percent undersaturated solution was injected beneath the mount to dissolve the crystals there. The position of the curve during the period of rapid growth rate in which the solution under the mount was crystallizing is not given. After the apparatus was dismounted, crystallization other than that attributed to the injected solution was not found, so the final negative growth rate probably is due to dissolution of fibers

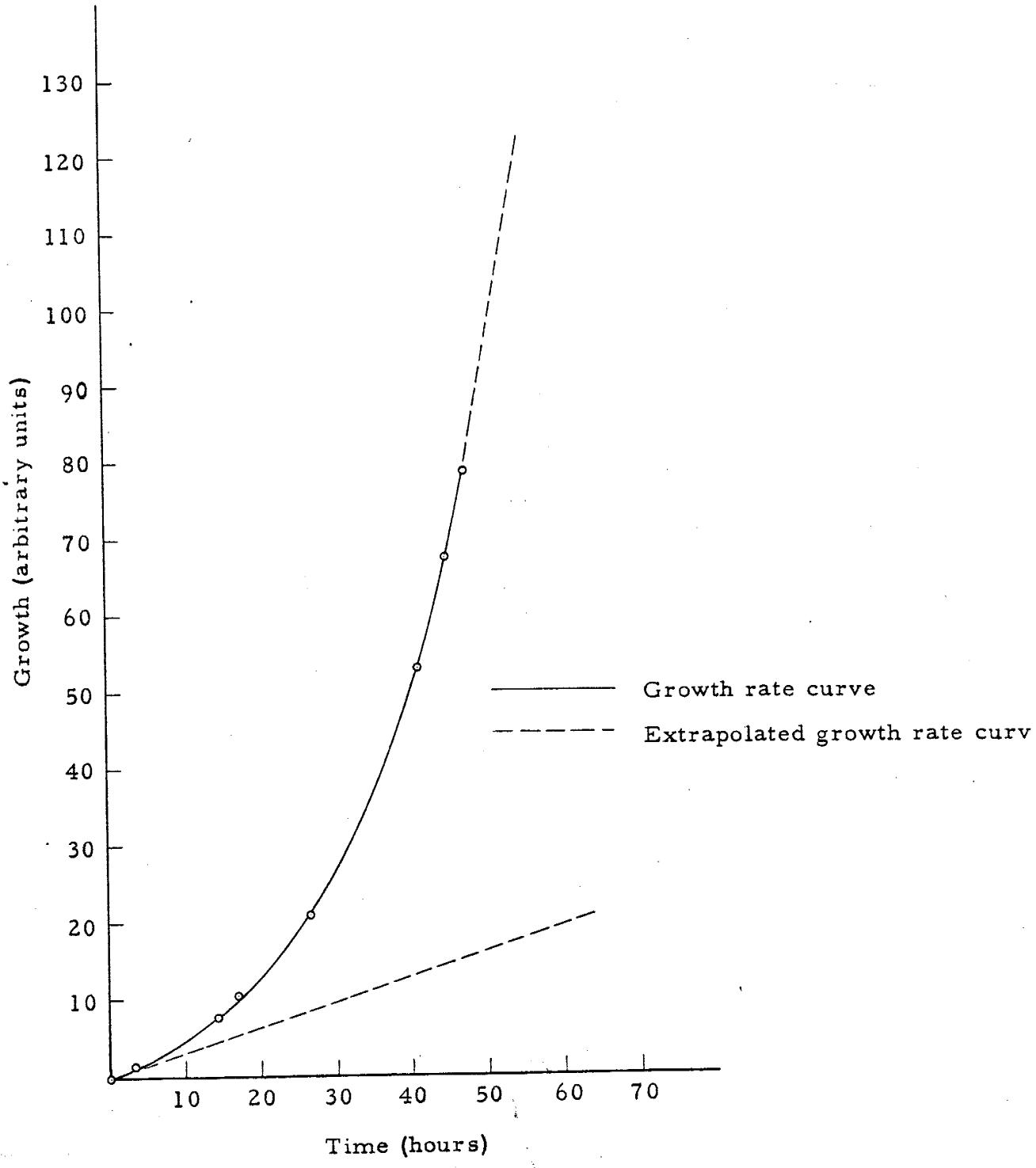

FIGURE 10. GRAPH OF GROWTH VS. TIME FOR RUN 1 OF ACB-3

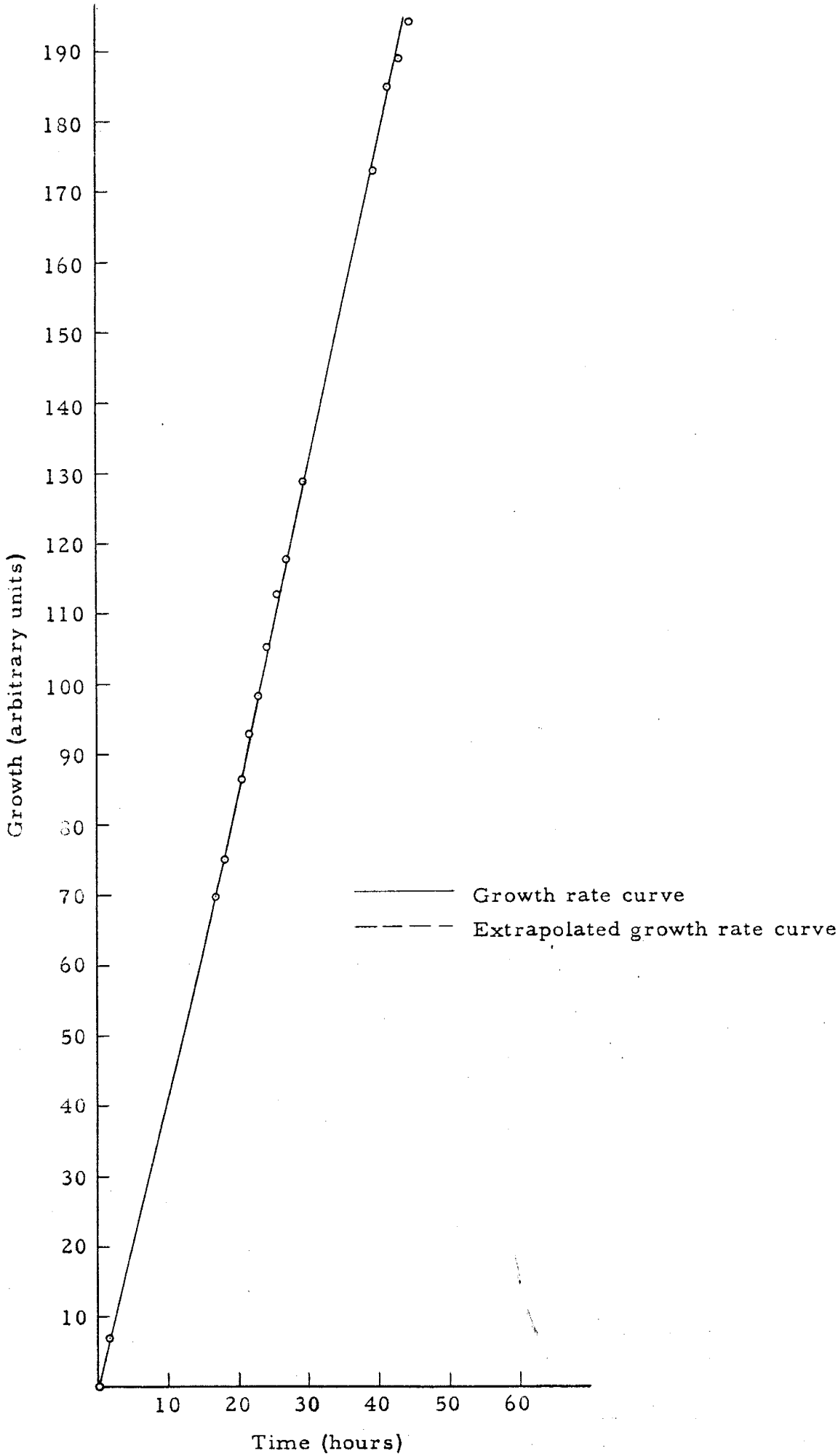
190
180
170
160
150
140
130
120
110
100
90
80
70
60
50
40
30
20
10
Growth (arbitrary units)
10
20
30
40
50
60
Time (hours)
Growth rate curve
Extrapolated growth rate curve

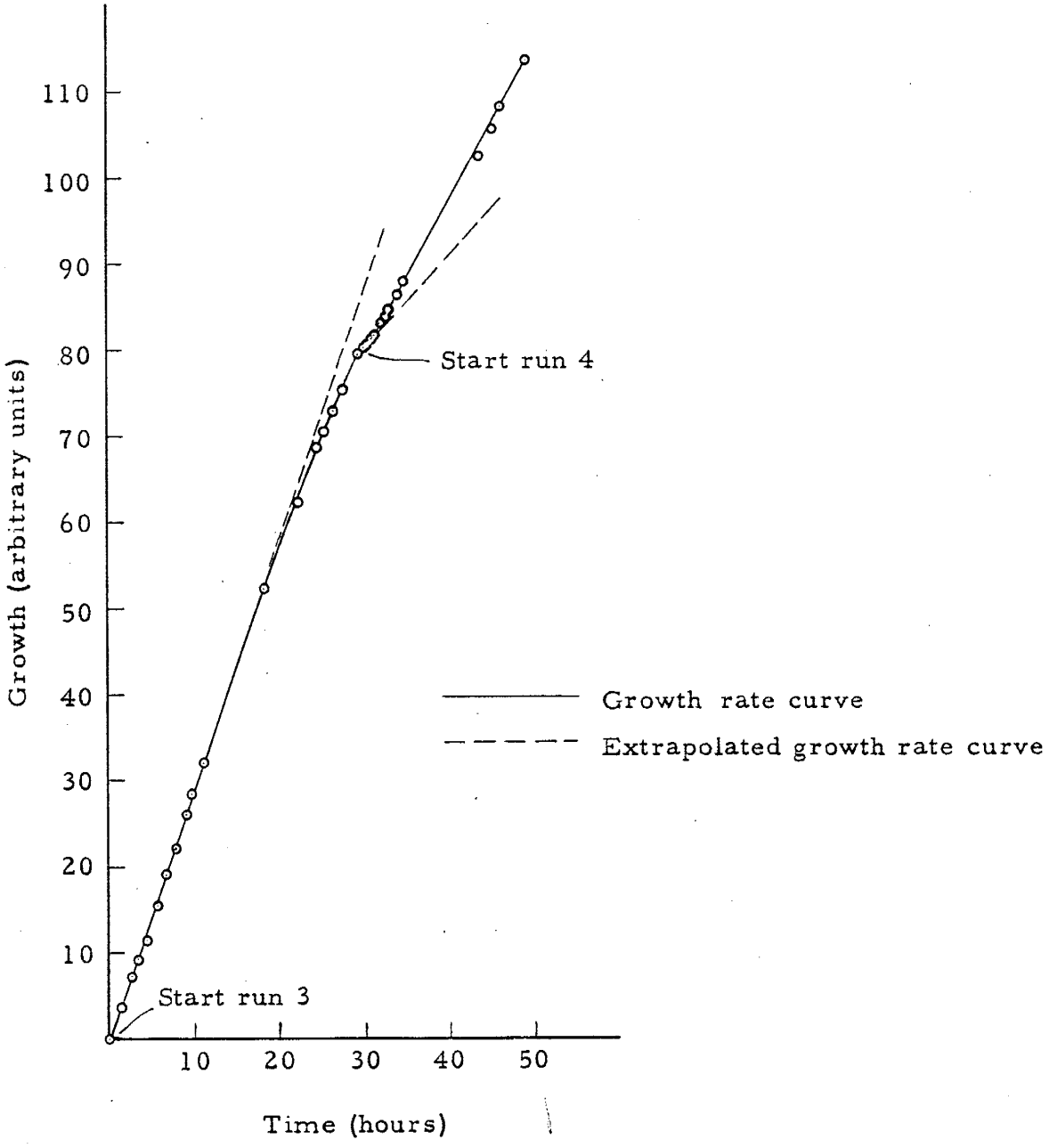

FIGURE 12. GRAPH OF GROWTH VS. TIME FOR RUNS 3 & 4 OF ACB-3

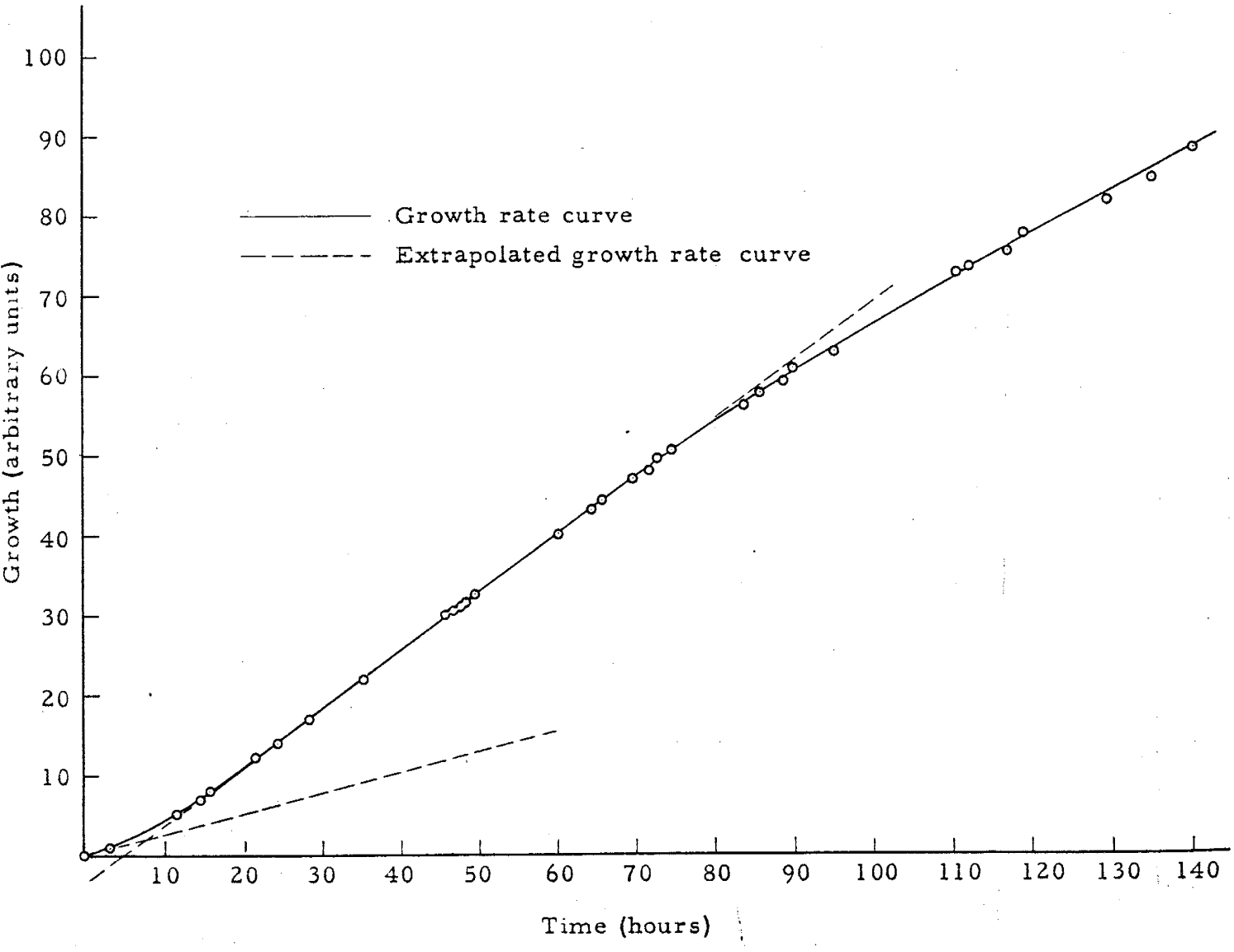

FIGURE 13. GRAPH OF GROWTH VS. TIME FOR RUN 5 OF ACB-3

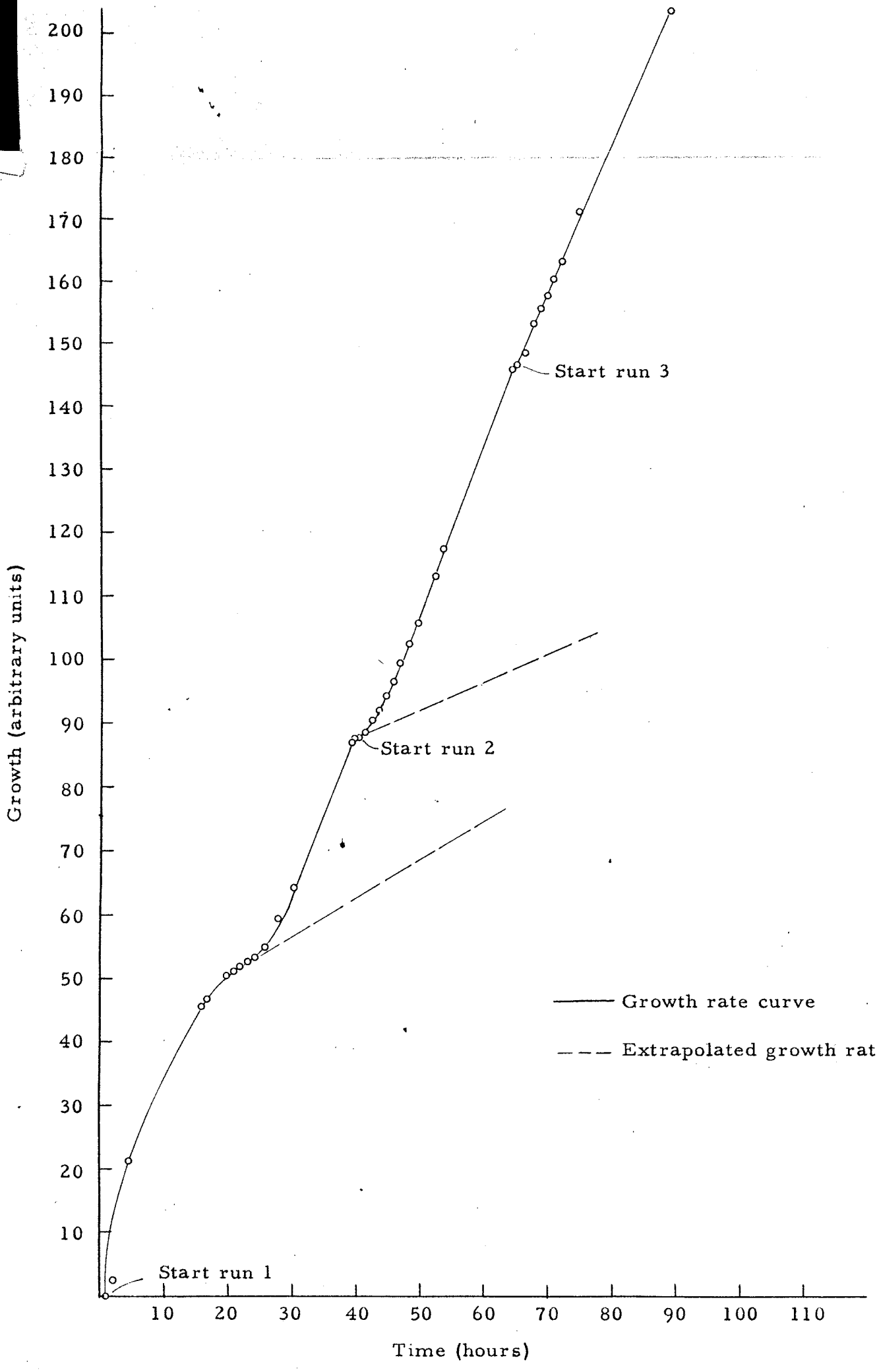

FIGURE 14. GRAPH OF GROWTH VS. TIME FOR RUNS 1, 2, & 3 OF ACB-8

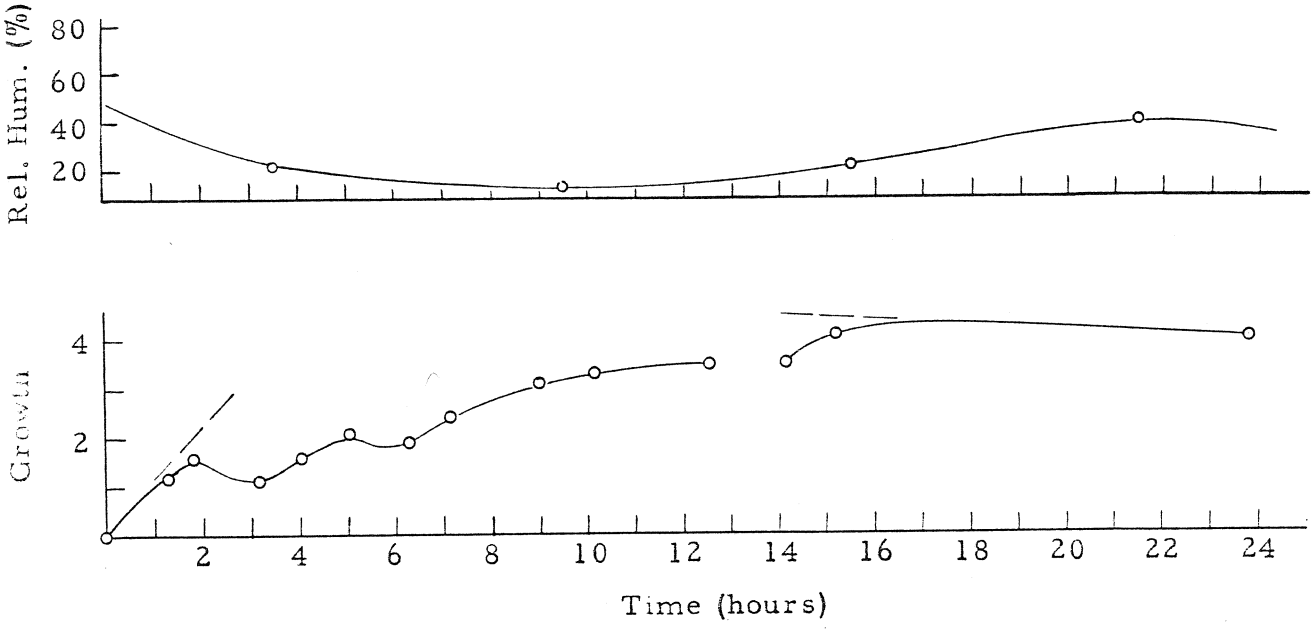

FIGURE 16. GROWTH AND RELATIVE HUMIDITY VS. TIME FOR RUN 5 OF ACB-8

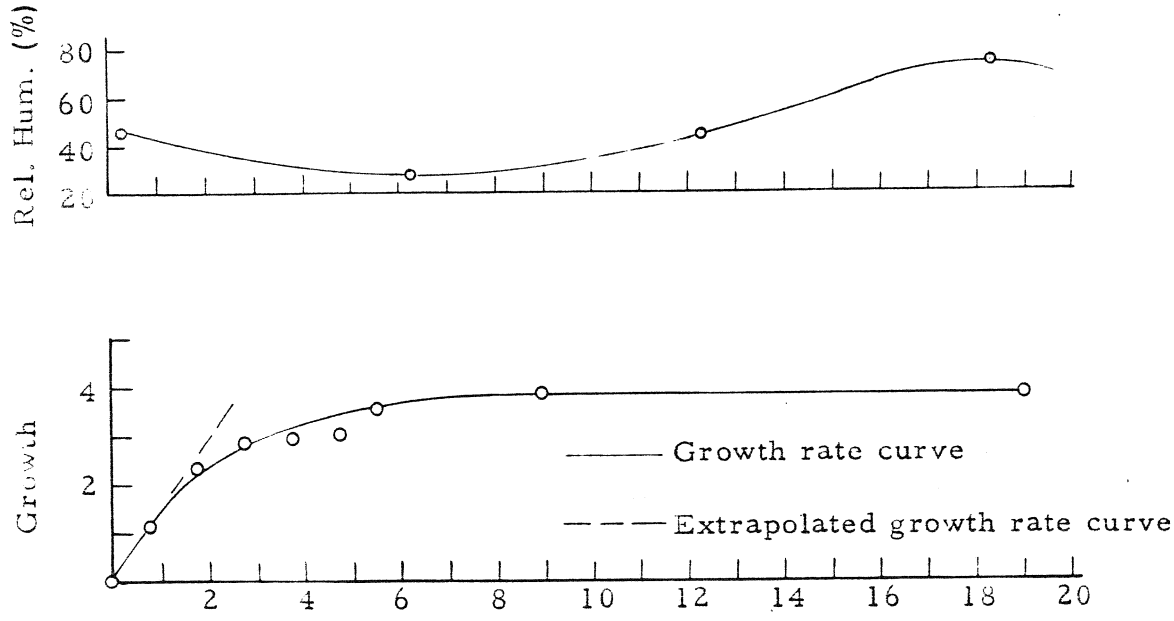

the concentration of the solution in the ceramic.

Meterologic effects on the growth rate

At pressure values of P_n near the maximum pressure the growth rate can be expected to be sensitive to small changes in the evaporation rate. In order to evaluate this, the percent relative humidity versus time was plotted opposite the growth values for runs 4 and 5 of ACB-8 in figures 14 and 15. As the humidity increases, the evaporation rate decreases and the growth rate should decrease also. The negative growth rates at the beginning of run 5 cannot be correlated with a decrease in evaporation rate. The zero growth rate at the end of run 4 and the negative growth rate at the end of run 5 do occur during periods of rising humidity; however, where the magnitude of the increase in humidity is greater at the end of run 4, the decrease in growth rate is greater at the end of run 5. This indicates that the negative growth rate at the end of run 5 and the zero growth rate at the end of run 4 are not the result of fluctuations in humidity.

Another factor which could be expected to affect the growth rate is temperature. The solubility of NaCl increases with temperature from 35.84 g/100 g H_2O at 15.20°C to 36.20 g/100 g H_2O at 30.05°C (Seidell, 1940). Although the change in solubility is not linear, within this range it is nearly so, and one can estimate a

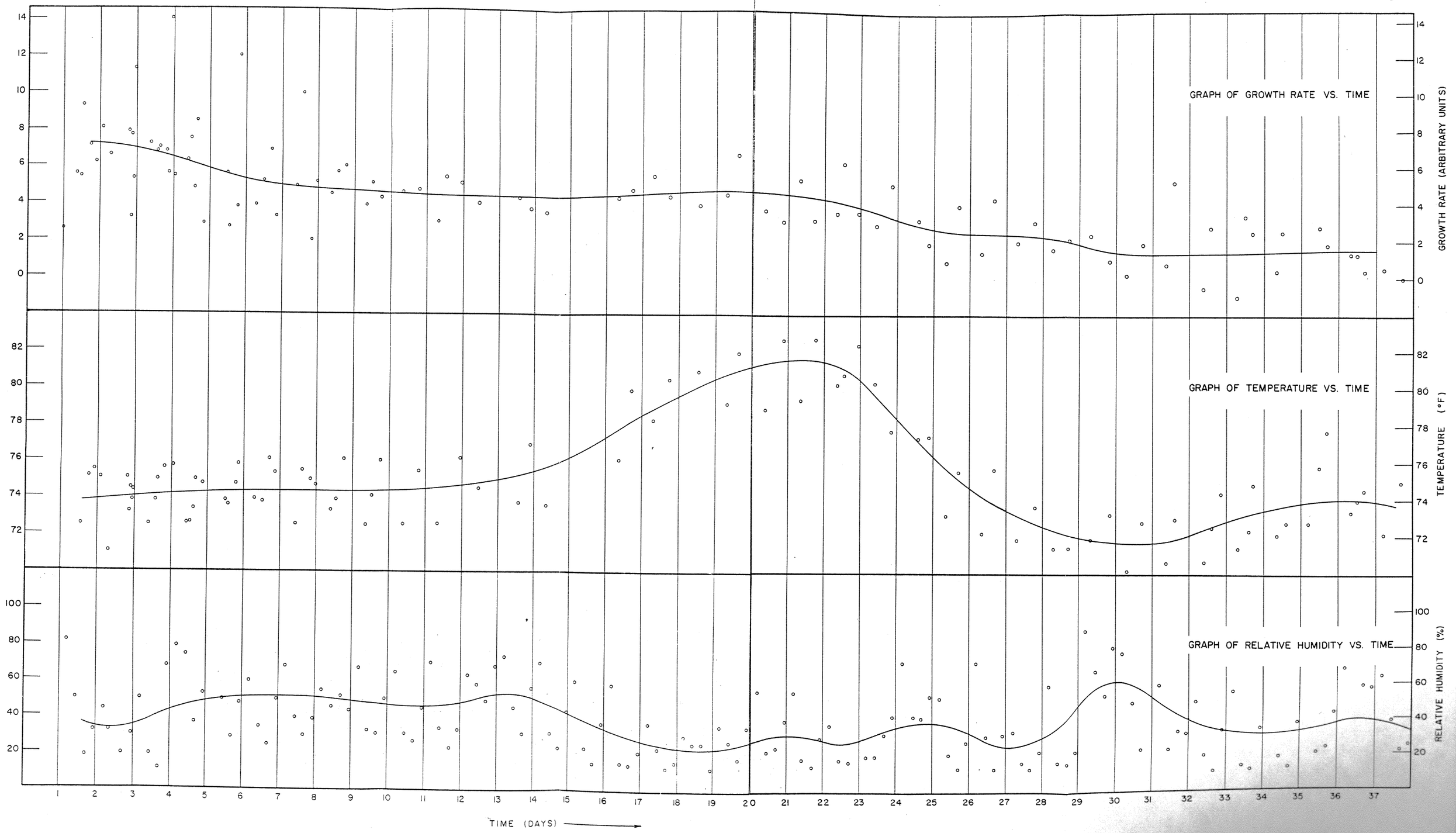

FIG. 17. CORRELATION OF GROWTH RATE WITH TEMPERATURE AND RELATIVE HUMIDITY

The growth rate should then be expected to decrease as the temperature increases.

Both temperature and percent relative humidity were plotted against growth rate for the duration of run 5 of ACB-3 in order to determine if there were any long range atmospheric effects on the growth rate (see figure 16). Temperatures were measured in the laboratory and humidity data were supplied from the weather station on the N. M. I. M. T. campus by Dr. Wilkening. Spot checks with humidity measurements in the laboratory were in close agreement.

During run 5 of ACB-3, there is a general decrease in the growth rate with time which is probably due to approaching exhaustion of the solution in the mount. In effect, as the solution in the mount is used up, diffusion becomes less efficient, fibers may lose contact with solution, and the growth rate drops off. However, there is a conspicuous leveling off of the growth rate after the 15th day which is coincident with a prominent rise in the estimated mean temperature and a decrease in the estimated mean humidity of roughly one-half. With subsequent decreases in the temperature and increases in the humidity after the 28th day, the growth rate again decreases. It then levels off with a decrease in humidity and a slight increase in temperature after the 32nd day. These data indicate that the growth rate is relatively insensitive to temperature effects at least under the experimental conditions, but that there may be slight effects due to changes in humidity. Daily variations in humidity do not appear

to have a measurable effect. The short term measurements involved in the determination of the maximum growth pressure appear to be relatively free from meteorologic influences.

Determination of maximum growth pressure from stress and growth rate measurements

It is evident from the preceding pages that a correlation exists between the stress of a crystal and its growth rate. If the growth rate is plotted against the logarithm of the pressure, as in figure 19, a linear curve results. In figure 19, three curves are drawn. The dashed line is merely drawn through four points at 19.7, 16.1, 11.5, and 7.40 bars. The dash-dot line was determined by the method of least squares and includes the value of 24.6 bars. It crosses the pressure axis at 24.0 bars. The solid line was also determined by the method of least squares and includes the value of 31.2 bars in addition to 24.6 bars. It crosses the pressure axis at 24.9 bars. The author considers the dash-dot line to be the most valid.

It is apparent that given sufficient growth rate and stress measurements, the maximum growth pressure can be determined graphically. However, it is important to know if the maximum growth pressure can be determined from only one set of rate and

stress measurements. Toward this end, an expression was derived for P_m in terms of the stress on a crystal and its growth rate.

The empirical relation of Chrétien et al (page 20) may be written as

$$r = a \left(\frac{c}{c_s} - 1\right)^2 \times 10^4$$

where

r = growth rate
a = constant of proportionality carrying the units of rate
c = prevailing concentration of the solution
c_s = concentration of the saturated solution as determined by the solubility of the unstressed crystal

If the crystal is stressed, its solubility will increase and the effective supersaturation will decrease. We can then say that the growth rate, r_1, for a crystal growing under a pressure of P_1 will be given by

$$r_1 = a \left(\frac{c}{c_1} - 1\right)^2 \times 10^4 \quad . \quad . \quad . \quad . \quad . \quad . \quad . \quad . \quad . \quad (1)$$

where c_1 is the solubility of the crystal growing under the given load. In both the unstressed and the stressed cases c is the same, so the growth rate will be less in the stressed case.

Correns' equation may be converted to the exponential form

$$e^{P_m/K} = \frac{c}{c_s}, \quad \text{where } K = \frac{1}{V} RT$$

and P_m = maximum growth pressure.

This is an equilibrium equation and dividing by the equilibrium equation for P_1 (which is less than P_m) gives

$$\frac{e^{P_m/K}}{e^{P_1/K}} = \frac{c/c_s}{c_1/c_s} = \frac{c}{c_1} .$$

From equation (1) the growth rate at P_1 is given by

$$r_1 = a \left(\frac{e^{P_m/K}}{e^{P_1/K}} - 1\right)^2 \times 10^4 \quad . \quad . \quad . \quad . \quad . \quad . \quad (2)$$

Rearranging and taking natural logarithms,

$$(r_1/10^4 a)^{1/2} + 1 = \frac{e^{P_m/K}}{e^{P_1/K}}$$

$$e^{P_m/K} = e^{P_1/K} \left[(r_1/10^4 a)^{1/2} + 1\right]$$

$$P_m/K = P_1/K + \ln \left[(r_1/10^4 a)^{1/2} + 1\right]$$

$$P_m = \frac{1}{V} RT \ln \left[(r_1/10^4 a)^{1/2} + 1 + P_1\right] . \quad . \quad . \quad (3)$$

According to Chrétien et al (1954, a is a constant. If this is true for crystal growth under stress, then the determination of a will permit calculation of P_m from only one set of stress and growth rate measurements. To this end, a's were calculated from equation (2) and plotted against the logarithm of P_m in figure 18. The curve was determined by the method of least squares. The data suggests that a varies with P in a regular manner.

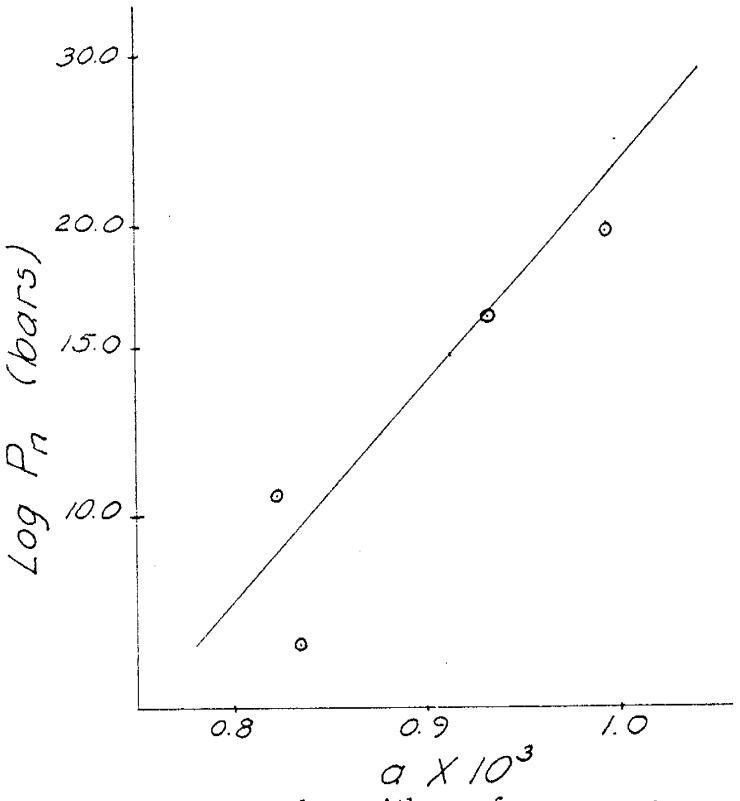

Figure 18. a versus logarithm of pressure

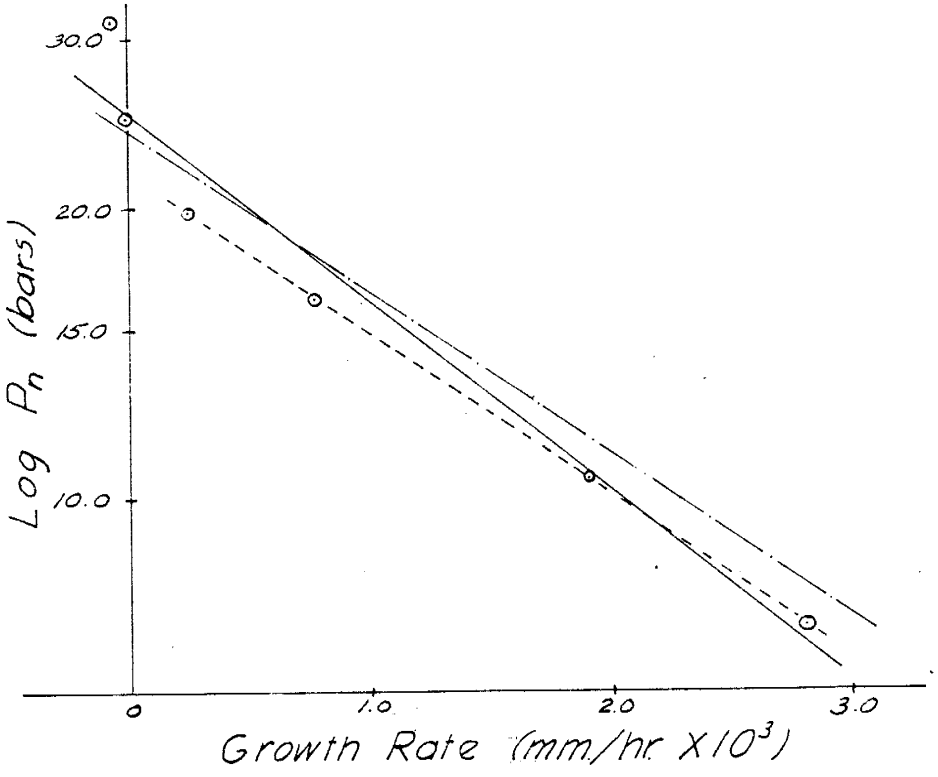

Figure 19. Growth rate versus logarithm of pressure.

Equation (3) was solved for P_m by using various values of a. A summary of the results are given in Table II. Averages are given with their standard deviations from the arithmetic mean. In the table, P_m (1) is calculated by using respective a's determined from equation (2). P_m (2) is calculated by using the average of the a's calculated from equation (2). P_m(3) is calculated by using a's determined from the straight line of figure 18.

The P_m(3) values agree most closely with the measured value of P_m. They indicate that the variation of a with the logarithm of P_n is significant.

In the Chrétien investigation, the concentration of the solution was varied in order to investigate growth rate while the solubility of the crystals remained constant. However, during the present investigation, the concentration of the solution remained constant while the growth rate changed due to the varying solubility of the crystals under stress. Apparently a is not a constant when crystals grow under stress. The fact that a is constant in the unstressed state and variable in the stressed state means that amongst others, it is a function of the solubility of the mineral.

An analytical expression for a in terms of solubility was not found. Lacking such an expression, equation (3) cannot be solved with knowledge of only one set of stress and growth rate measurements or without prior knowledge of P_m.

TABLE II. SUMMARY OF CALCULATED DATA

Sample	Run	$a \times 10^3$	$P_m(1)$ bars	$P_m(2)$ bars	$P_m(3)$ bars
ACB-3	4	0.822	24.7	24.0	24.5
	5*	0.993	24.6	24.6	24.7
	5	0.931	24.6	24.8	24.6
ACB-8	2	0.834	23.4	24.2	25.0
Averages		0.895 ± 0.091	24.3 ± 0.3	24.4 ± 0.2	24.7 ± 0.1

*calculations are based on data obtained at the beginning of run 5.

Summary of growth pressure investigation

A measurable growth pressure was found to exist for NaCl fibers in equilibrium with a saturated salt solution. This pressure was found to be of the order of magnitude of 25 bars. It was found that considerably higher pressures than that which was measured directly could exist, but that the solution under these conditions was highly metastable and its concentration soon decreased to that consistent with a lower pressure.

The effects of temperature and humidity were examined and their daily fluctuations found to have no significant effect on the growth rate of the fibers. Changes in relative humidity were found to have a slight effect on the growth rate over a period of several days but only as the solution in the mount neared exhaustion. A decrease in daily mean relative humidity causes an increase in growth rate as would be expected.

CRYSTALLOGRAPHY OF THE ARTIFICIAL NaCl FIBERS

In order that the growth mechanism of salt fibers could be better understood, a series of X-ray diffraction patterns of the fiber aggregates was obtained. It was desired to determine if a preferred orientation of the fibers existed, and if so, the degree of parallelism of the component fibers.

X-ray diffraction patterns were obtained in a Norelco powder camera and a Laue camera constructed by Dr. M. S. Sun, mineralogist of the New Mexico Institute of Mining and Technology. The orientation of the fiber axes as mounted in the cameras is given in Table III. In all pictures copper K_α radiation was used. The A. S. T. M. Powder Data File was used to index the reflections.

Determination of fiber orientation

Data obtained from the powder camera and Laue camera pictures were analyzed by means of pole figures to determine the fiber axis and preferred orientation. In constructing the pole figures, the fiber axis is first plotted as the North-South axis of a stereogram, and the poles of the various reflecting planes are plotted stereographically in the same azimuthal positions that their respective reflections occupy on the X-ray film. The angular deviations (rho values) of the poles of the reflecting planes from the fiber axis can then be read from the

stereonet. In the case of a fibrous cubic mineral with a perfect [100] fiber axis, the rho values of the poles for 200 and 111 reflecting planes will be $90^{\circ}00'$ and $54^{\circ}44'$ respectively. When the fiber orientation is imperfect (as is the case with the fibers grown during this investigation), it is necessary to plot the rho values on a standard stereogram of the fiber's crystal system. The rho values are plotted as small circles, and the intersection of the circles for three different reflecting planes defines a possible fiber axis direction.

The directions of possible fiber axes (F.A.) for the fibers grown during this investigation were plotted according to the method explaned above and are given in figures 20-22. In most cases the small circles did not intersect in points, but as triangles of error. The centers of the triangles of error were taken as possible fiber axis directions. The lack of perfection in the orientation (subparallelism) enabled several fiber axis directions to be plotted from a single diffraction pattern (figure 22) or from a pair of patterns (figure 20). The fiber axis directions indicated on figures 20 and 21 strongly suggest an imperfect [100] orientation. Figure 22 shows that [027] may be a fiber axis direction; however, the high symmetry of NaCl should permit only [100], [110], and [111] directions as true fiber axes. The occurrence of intersections defining other than one of these directions is taken as representing lack of parallelism of the component fibers and/or

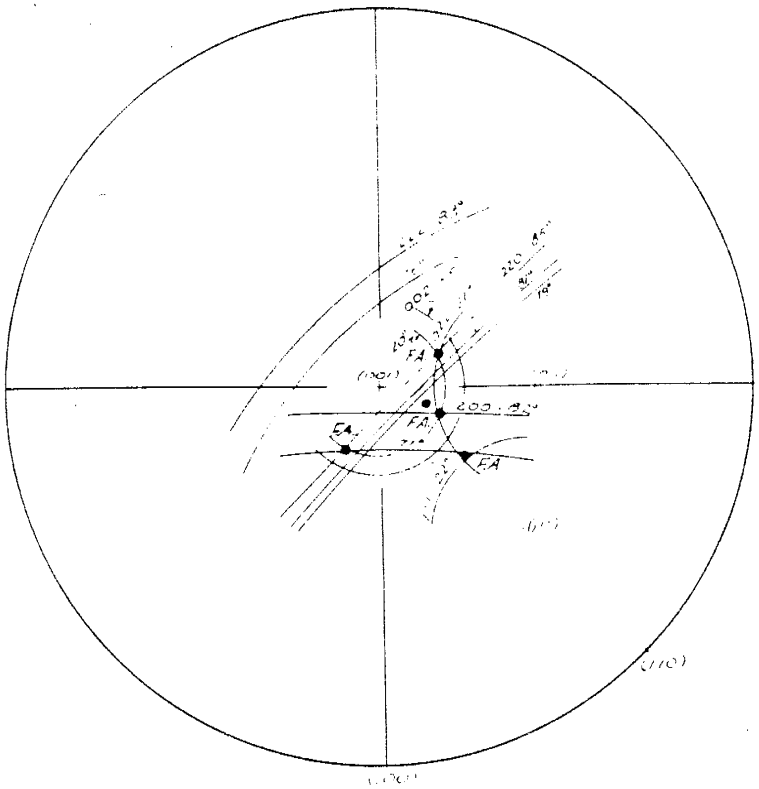

Figure 20. Stereogram of possible fiber axes constructed from powder pictures nos. 13 and 14. Indicated angles are the deviations of the respective reflections from the F. A.

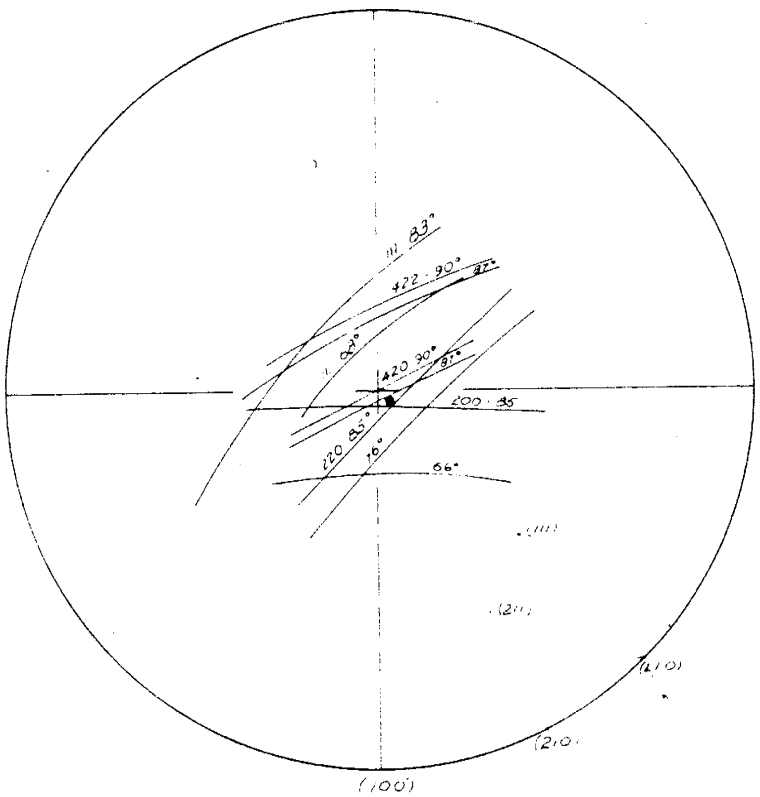

Figure 21. Stereogram of possible F. A. constructed from powder pictures nos. 7 and 11. Angles are as above.

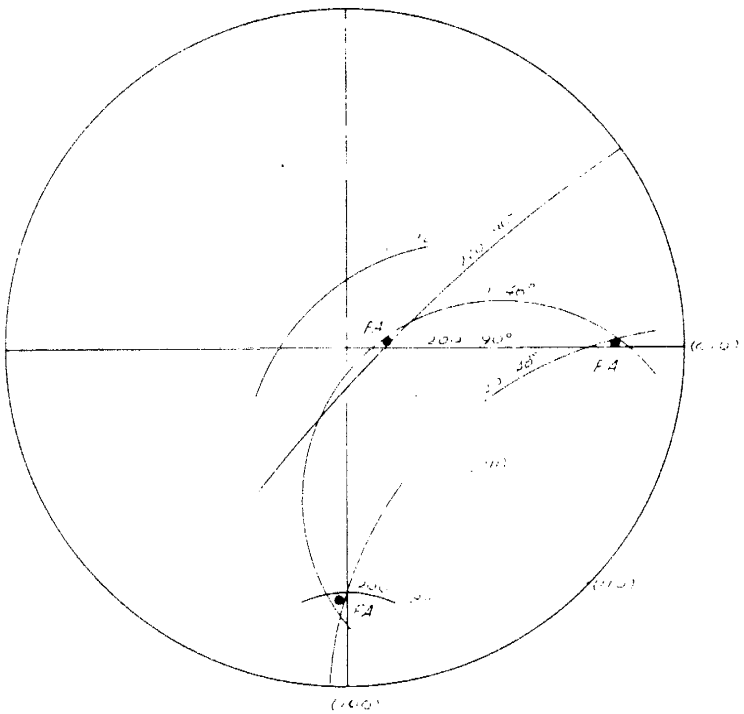

Figure 22. Stereogram of possible F. A. constructed from Laue picture no. 19. Angles are as in figure 20.

curvature in the fiber sample when it was X-rayed. The aggregates are extremely difficult to handle for mounting in the camera and spurious reflections undoubtedly occur from broken fibers and adhering salt fragments.

A qualitative idea of the degree of randomness in the fiber orientation can be gained from Laue diffraction pattern no. 19 (figure 23). An almost complete Debye ring representing the 200 reflecting planes is present with scattered intensity maxima. The 200 reflection maxima represent a certain amount of non-parallelism of the component fibers of the fiber aggregate as well as broken fibers and adhering salt fragments. The 220 reflection maximum in the lower left corner and the 111 reflection maxima are consistent with an approximate [100] fiber axis direction. The 220 and 111 reflections carry more weight than the 200 in deciding on a preferred orientation of the NaCl fibers because their intensities are much weaker than that of the 200 reflection.

The existence of a preferred fiber orientation is better shown by Laue diffraction pattern no. 30 (figure 24). This pattern was taken when the fiber spindle was tilted out of vertical and away from the X-ray source by an angle equal to the Bragg angle (15.84°) of the 200 planes for Cu Kα radiation. It is seen that the 200 reflection maxima occur predominantly in the lower portion of the Debye ring. This indicates that the [100] is the fiber axis of the aggregate. The lower 220

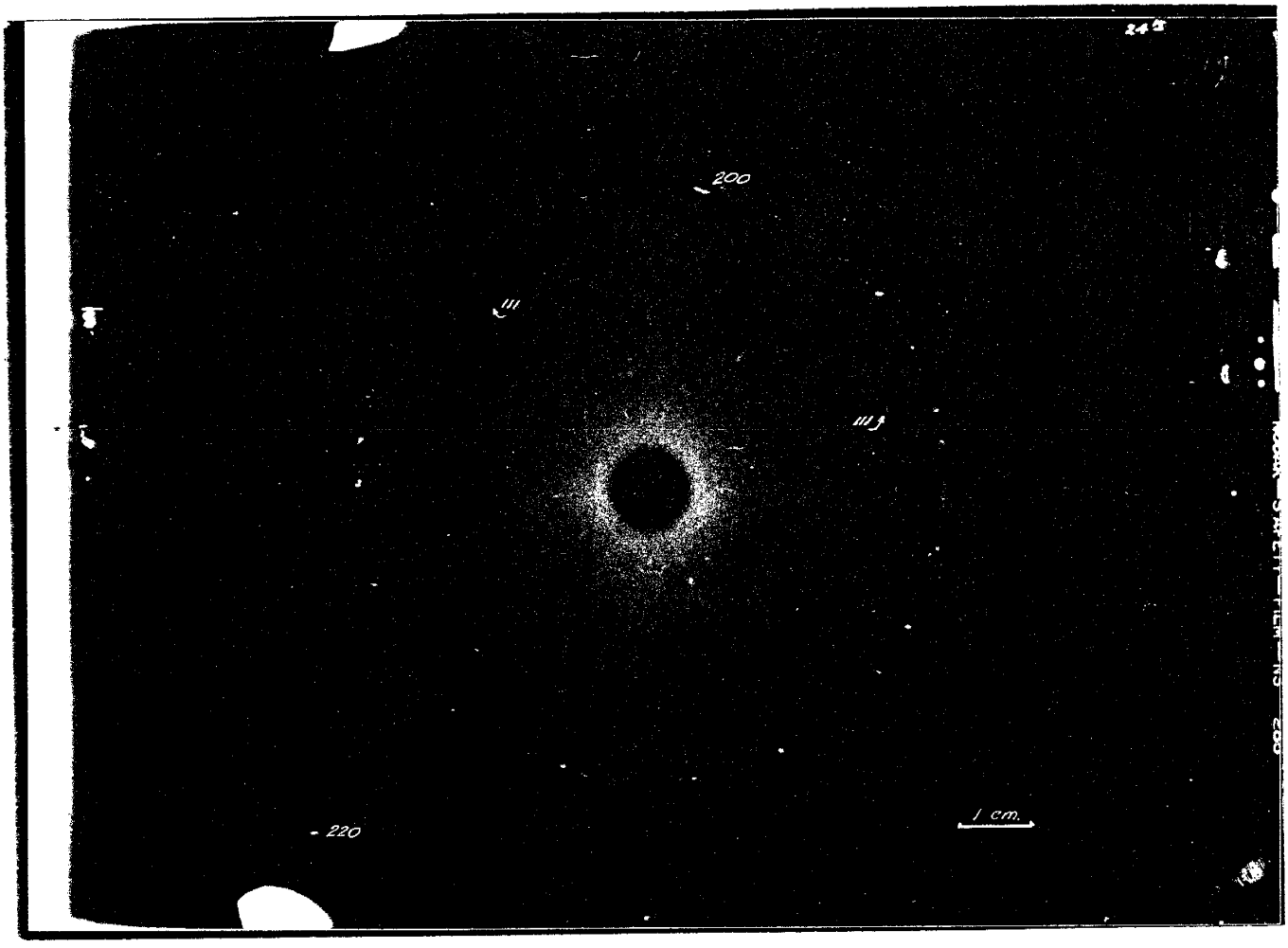

Figure 23. Laue picture no. 19. Crystal-film distance is 6.637 cm. The photo is a contact print made from the X-ray film.

spot and the 111 spots are consistent with a [100] fiber axis orientation. The bright 200 spot on the right side of figure 24 and the upper two 220 spots indicate that many crystals in the aggregate do not have a preferred orientation. Again, the intensity maxima at angles less than the Bragg angle for the 111 planes are due to continuous radiation.

Theoretical work by Kamb (1959) on preferred orientation of crystals subjected to uniaxial stress indicates that the [100] direction of NaCl should become aligned parallel to the principal stress direction. His work indicated that for a cubic crystal, stable orientation is always attained with the crystallographic axes either parallel or perpendicular to the maximum or minimum stress direction in a uniaxial stress field. The fibers grown in this investigation have attained an orientation which is consistent with Kamb's work.

Determination of the amount of fiber subparallelism

It is apparent from the preceding discussion that a certain lack of parallelism exists between the component fibers of a fiber aggregate. It was desired to evaluate quantitatively this subparallelism, and to this end a method using the normal intensities and observed intensities of the various reflecting planes was devised.

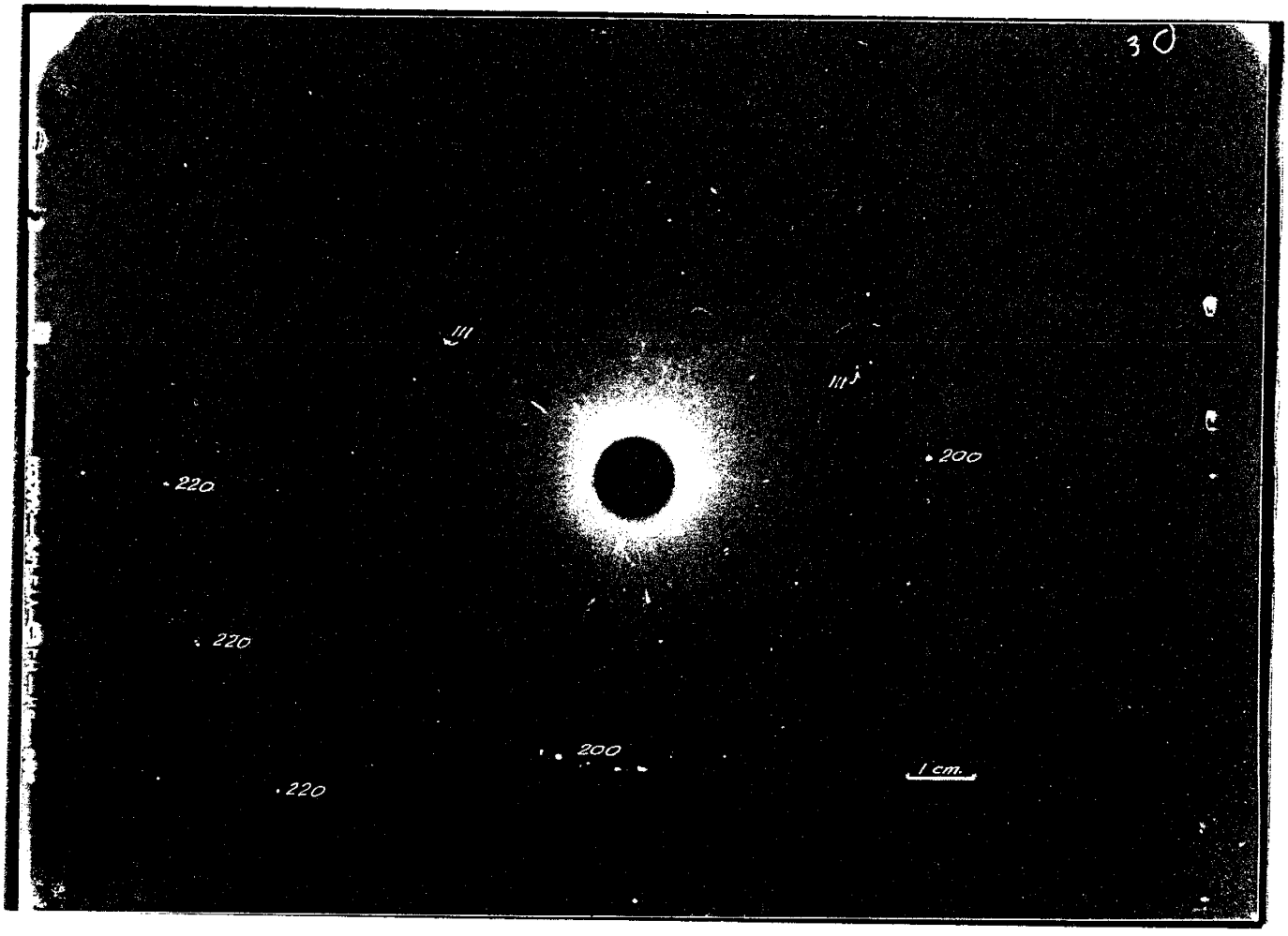

Figure 24.. Laue picture no. 30. Crystal-film distance is 6.637 cm. The photo is a contact print made from the X-ray film.

If all of the fibers in a fiber aggregate have a common parallel crystallographic direction, an X-ray beam directed down the fiber axis will give reflections from only those planes whose crystallographic angles with the fiber axis satisfy Braggs Law. In the case of an aggregate of subparallel fibers where A is the angle between a constituent fiber's axis and a plane hkl, and that plane gives a reflection at the Bragg angle of θ_{hkl}, then the fiber's axis deviates from the X-ray beam by an angle equal to $A - \theta_{hkl}$.

If there are a sufficiently large number of fibers, the relative intensity of the various reflections will be proportional to the number of planes in reflecting positions. From this relationship, comparison of the intensities of the various reflections gives an indication of the relative abundance of the various reflecting planes if the normal intensities of the reflections are taken into account. (Normal intensity is the intensity of reflections of a powder sample without any preferred orientation). Given the crystallographic angles A, the Bragg angles, and the intensities, the angular deviation of fibers from the composite fiber axis can be determined.

In the application of this method, diffraction pattern no. 8 (figure 25) was used. For this exposure, the fiber aggregate was

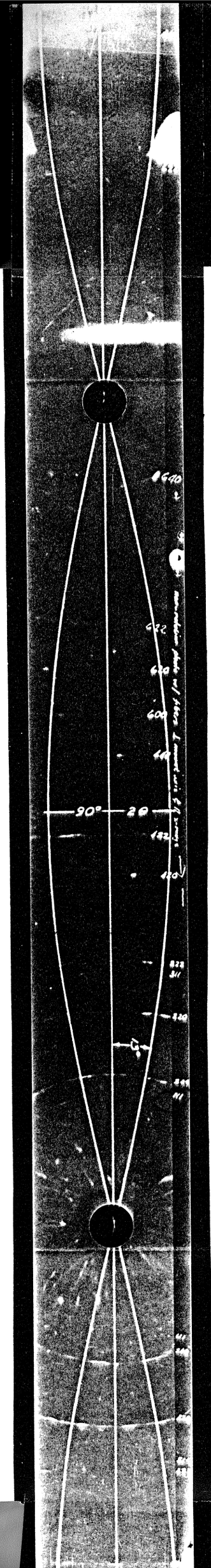

Figure 25. Powder picture no. 8. Cu K radiation with the fiber axis parallel to the X-ray beam. Picture is a contact print of the film.

mounted in a powder camera with the fiber axis parallel to the X-ray beam. All planes reflecting at an intensity of more than one percent of the normal 200 intensity (with the exception of the 444 and the 400) gave some reflections. The total energy falling on the film within an azimuthal interval of 52° as measured around the axis of the X-ray beam -- 26° is the angle intercepted by the film at $2\theta = 90^{\circ}$ -- was estimated for each set of reflecting planes and compared with the normal intensity ratios ($I/I_1 = 100$ for the 200 planes). The intensity of a very bright spot of one of the 420 reflections was chosen as 100 and the relative intensities of all other spots were estimated with respect to this one. The observed intensities were then reduced to ratios with the observed intensity of the 200 plane and then each divided by the normal intensity ratio for each respective plane in order to determine an intensity deviation factor. If the observed intensities had shown the normal relationship to one another, the deviation factors would all have had had values equal to 1.

The data of the relative ratios of intensity are tabulated in Table IV. In the table, A_1, A_2, and A_3 are the interfacial angles between hkl and $[100]$, $[010]$, and $[001]$ respectively. The reflecting plane is hkl and θ_{hkl} is the Bragg angle for the reflecting plane when Cu Kα radiation is used. Crystallographic data are from

Palache, Berman, and Frondel (1944) and the normal intensity ratios, with the exception of the 640 reflection, are from the A.S.T.M. X-ray Powder Data File.

It is apparent that the 440, 420, and 422 reflections have intensities 18.0, 8.3, and 8.0 times their normal intensities as indicated by the deviation factors given in the table. Furthermore, the 440 planes require a rotation of only 5.59° to bring them into a reflecting position if the fiber axis is [100]. It is necessary to rotate the 442 and 420 planes 8.76° and 11.10° respectively in order to bring them into reflecting positions. Other planes with $A_n - \theta_{hkl}$ less than 11.10° are 622, 640*, 313, 531, and 533. These planes did not reflect at intensities significantly different from $I/I_1 = 1$. This could be due to randomness of orientation or because only 52° of azimuth could be compared for all reflections. 311, 531, and 533 have normal intensities of only 1 to begin with and are only obtained under the most ideal conditions. At any rate, the low deviation factors for all planes with $A_n - \theta_{hkl}$ greater than 11.10° suggests that departure from parallelism of fibers is not much greater than this angle.

---

* A word should be said about the presence of the 640 reflection. The indices of this plane were determined from the "d" spacing and the table of quadratic forms in Azároff and Buerger (1958). The normal intensity of the reflection was determined by inspection from a single crystal rotation picture taken in a powder camera and so does not necessarily apply to intensities determined by the powder method. Nevertheless, an order of magnitude is indicated.

Diffraction pattern no.	Sample no.	Camera	Fiber orientation in camera	Remarks
7	ACB-1	powder	parallel to camera axis	non-rotation
8	ACB-1	powder	parallel X-ray beam	non-rotation
11	ACB-1	powder	parallel camera axis	non-rotation
13	ACB-3	powder	parallel camera axis	non-rotation; fibers grown under a load of 16.2 bars
14	ACB-3	powder	perpendicular to camera axis and perpendicular to X-ray beam	non-rotation; fibers grown under a load of 16.2 bars
19	ACB-3	Laue	parallel horizontal circle axis and perpendicular X-ray beam	characteristic radiation, fibers grown under a load of 16.2 bars
30	1	Laue	15.84° from horizontal circle axis in plane of X-ray beam and horizontal circle axis	characteristic radiation

TABLE III. EXPERIMENTAL CONDITIONS OF X-RAY STUDY

TABLE IV. SUMMARY OF DATA FROM PICTURE NO. 8

hkl	Θ_{hkl}	A_n	$A_n - \Theta_{hkl}$	Normal I/I_1	Obs. I/I_1	Deviation factor
200	15.84	$A_1 = 00.00$	15.84	100	100	1.0
220	22.72	$A_1 = 45.00$	22.28	55	187	3.4
222	28.24	$A_1 = 54.73$	26.49	15	40	2.4
111*	13.68	$A_1 = 54.73$	41.05	13		
420	37.65	$A_1 = 26.55$	11.10	11	91	8.3
422	44.03	$A_1 = 35.27$	8.76	7	56	8.0
400*	33.11	$A_1 = 00.00$	33.11	6		
620	59.75	$A_2 = 71.57$	11.82	4	2	0.5
600	55.02	$A_2 = 90.00$	34.98	3	5	1.7
622	64.94	$A_2 = 72.45$	7.51	3	2	0.7
640	79.89	$A_3 = 90.00$	10.11	3	7	2.5
311	26.92	$A_1 = 25.23$	1.69	2	3	1.5
440	50.59	$A_1 = 45.00$	5.59	2	36	18.0
444*	71.11	$A_1 = 54.73$	16.38	2		
331*	36.53	$A_2 = 46.51$	9.98	1		
511*	45.20	$A_1 = 15.79$	29.41	1		
531*	53.90	$A_3 = 59.53$	5.63	1		
533*	63.52	$A_2 = 62.77$	0.75	1		

* No reflections were obtained from these planes.

THE GROWTH MECHANISM OF FIBROUS NaCl

Observed growth characteristics

Growth of NaCl fibers was explained by Schmidt in 1914 after he had observed salt fibers growing on clay. He suggested that if the size of the capillary openings in the clay were small enough, a seed crystal formed at the air-solution interface would not be able to settle farther into the solution and growth would occur at the bottom of each seed, thus forming a fiber. He verified the basal growth of the fibers by dying the tops of the fibers and observing that the dyed portion of the fiber was raised above the substrate and that no new growth appeared above the dyed portion. The author performed the same test by marking the fibers with india ink and the same results were obtained. The crystals were not externally loaded and growth occurred in a dessicator. Over a period of 35 hours, the growth rate was measured as approximately 25 μ/hr.

Examination of a fiber aggregate reveals very close packing of the constituent fibers. In fact, for the most part, adjacent fibers appear to be packed as closely as possible and no unoccupied space between fibers is observed. With this sort of fiber packing, Schmidt's hypothesis would demand a fiber diameter of the same order of mag-

nitude as the grain size of the substrate.

After fibrous growth had been in progress during some of the runs, new fibers were observed growing below the ceramic surface and bulging it upward (see figure 8). This would suggest that fibers formed at the meniscus of the solution in the capillary openings and that as the solution was gradually used up, crystals formed at lower and lower positions in the mount. Lowering of the solution would most likely occur where there had been no previous fibers, for fibrous growth at the air-ceramic interface would tend to maintain the solution at that level.

The author has observed that crystals which form in a freely evaporating solution are often formed at the surface and are held there by surface tension. The greater supply of solution below the crystals caused them to grow as platelets with the [100] direction normal to the air-solution interface.

Growth characteristics observed by Bunn and Emmett (1949) and the growth hypothesis of Kossel (1928) may be used to extend the hypothesis of Schmidt for fibrous NaCl. Bunn and Emmett observed and photographed with a movie camera layer by layer growth of NaCl crystals. The layers were observed to begin near the centers of (100) faces and progress rapidly toward the edges. They estimated the layers to be several hundreds of atoms thick. The model of ionic

crystal growth developed by Kossel is consistent with this observed behavior and entails the laying down of ions to complete atomic rows and planes. According to this hypothesis, once a row has been initiated by the deposition of an ion, its associated plane is rapidly completed. This is followed by a lull in the growth during which the concentration of the solution must rise to a level from which new ions may be deposited. If a supersaturated solution possesses a certain amount of order in the vicinity of the crystal surface and is, in effect, poised to crystallize, one would expect growth to occur by advancing layers several ions thick or even several hundred ions thick as observed by Bunn and Emmett.

Suggested growth mechanism of fibrous NaCl

From the behavior of growing NaCl crystals discussed above, the growth mechanism of fibrous NaCl is considered by the author to be as follows. 1) Upon removal of the mount from the solution in which it soaked, the solution wetting the surface at the ceramic-air interface is removed by rapid crystallization of a salt crust composed of randomly oriented salt cubes. This rapid crystallization will form crystals too large to grow into fibers. 2) As the surface of the solution begins to recede below the top of the ceramic grains at the air-ceramic interface, new crystals

form with (100) faces parallel to the solution meniscus. 3) During lateral growth, the seed crystals encounter the inward sloping surfaces of ceramic grains defining the capillary opening which at the level of the crystal's base has the shape of a cup (see figure 26). 4) Advancing layers on the base of the crystal try to complete their associated atomic planes and when they reach the surfaces of the confining ceramic grains, force the crystal upward, and thus remove its upper portion from contact with the solution. 5) As the crystal grows upward, its base will tend to grow laterally until it either encounters another fiber, or runs out of solution. The arresting of lateral growth by lack of solution can be expected to occur near the top of a confining grain, for if adjacent capillary openings contain solution, they would also probably be growing fibers, as the concentration in two adjoining capillary openings will be very nearly the same. Should the base of a fiber extend into an adjacent capillary opening by creeping over a wetted confining grain, the increased supply of solution within the adjacent capillary opening could automatically cause the growth of a new crystal connected at first to the parent one. With high degrees of supersaturation, Kern (1953) reported (110) dendritic growth on the $\{100\}$ form of NaCl crystals. Such dendritic growth could extend into neighboring capillary spaces, and initiate the growth of new crystals. 6) As growth continues,

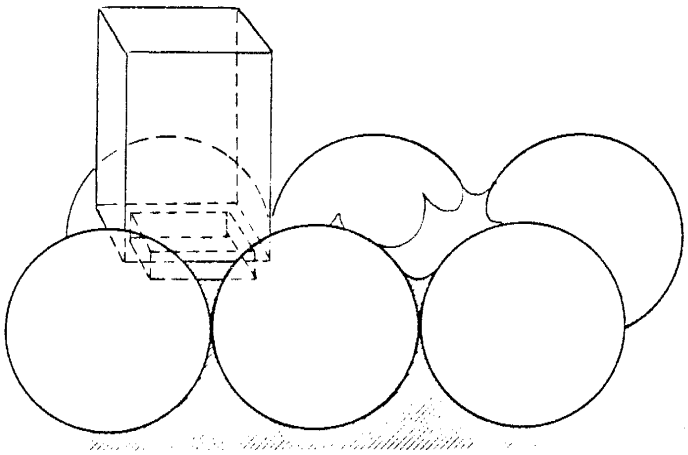

Figure 26. Schematic diagram showing a fiber seated between three equilaterally packed ceramic grains. At the base of the fiber is an advancing growth layer. The cross-hatched area is a cross-section of the solution within the capillary pores.

fibers will grow closely packed with a [100] orientation. Loading will, as Kamb (1959) predicted, tend to perfect the preferred [100] orientation, and as the author has observed, increase the density of fiber packing.

The ability of the solution to gain entrance between the base of the growing crystal and the confining ceramic grains is of considerable importance, for crystallization would not take place at the crystal-ceramic interface if solution was not available there. The entrance of solution between the crystal and ceramic grain is dependent on the phase boundary surface energies and the condition

for entrance of solution between crystal and substrate is given by Correns (1949) as

$$\sigma_{ac} > \sigma_{ab} + \sigma_{bc} \quad \ldots\ldots\ldots\ldots \quad (4)$$

In this expression σ_{ac} is surface energy between the substrate, a, and crystal, c; σ_{ab} is the surface energy between the substrate and the solution, b; and σ_{bc} is the surface energy between the solution and the crystal.

According to Correns the phase boundary forces contribute to differences in growth pressure as measured on different faces of alum; however, he states that the existence of unstressed faces is also important, as was mentioned earlier.

Surface energy also has an important influence on the lifting mechanism of fibrous crystal growth and on fiber orientation. Herring (1952) gives good theoretical and experimental evidence showing that the (100) faces of NaCl crystals have much lower surface energies than the other possible faces. Thus a growing salt crystal would have a strong tendency to maintain its cubic symmetry and not permit the existence of stepped surfaces as illustrated in figure 26. The existence of several such steps would define a plane of higher indices than 100 and would not be in keeping with the minimum surface energy necessary for equilibrium. The upper portion of the crystal

then would be lifted from the solution by the tendency for the crystal to eliminate those steps.

From the inequality (4) one can say that as σ_{ac} increases, the ease with which solution can enter between substrate and crystal increases. Thus a salt crystal oriented with its (100) face parallel to the solution meniscus and, say a possible (110) face tangent to a confining grain would grow less tightly against the confining grain, than a crystal with its (100) plane oriented tangent to the confining grain. The increased supply of solution to the first crystal would give it an advantage in growth and tend to perfect a $[100]$ fiber orientation.

GEOLOGIC IMPLICATION OF THIS INVESTIGATION

Introduction

Taber in 1916 experimentally produced cross-fiber veins of copper sulfate and alum in the laboratory by essentially the same procedure followed in this investigation. From his results and from field evidence of cross-fiber veins of gypsum, calcite, and asbestos, he concluded that these veins form by a process of lateral secretion. Cook (1936) followed up Taber's hypothesis in his description of the Thetford asbestos deposits in Quebec and suggested, in agreement with Taber, that the growth pressure of fibrous crystals was sufficient to dilate the fractures in which they grew. Experimental evidence of the existence of the growth pressure of fibrous NaCl supports this view and it was desired to study natural occurrences of fibrous halite if they could be found. To this end the salt deposits at the Zuni Salt Lake were examined.

Zuni Salt Lake (see figure 27) lies in western New Mexico about 19 miles northwest of Quemado on State Highway 32. The author is indebted to Mr. J. Sedillo, foreman of the Curtis Salt Co. for permission to collect samples at the lake. Zuni Salt Lake lies in a Quaternary collapse structure (Mr. Max Willard, personal communication) which is about 1.5 by 1.2 miles in diameter. The

lake is 0.7 by 0.5 miles in diameter. Within the structure are four smaller cinder cones with the largest containing a crater pond 175-200 feet in diameter. The pond is at the same elevation as the lake. The volcanic rocks are pyroclastic olivine basalts and the walls of the collapse structure are composed of Cretaceous sandstones and shales assigned to the Mancos shale formation (Willard and Weber, 1958).

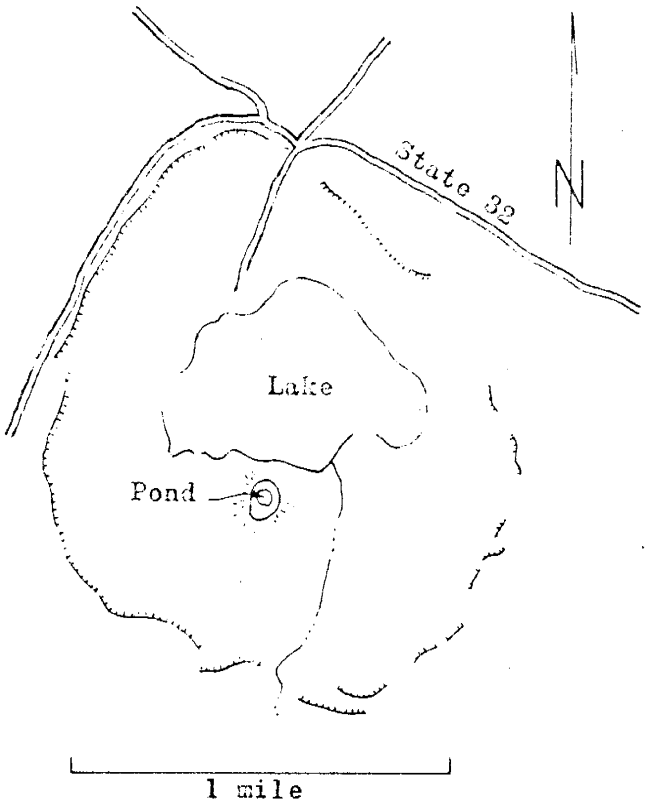

Figure 27. Map of Zuni Salt Lake. Data from Soil Conservation Service (New Mexico Quad 241).

Darton in 1905 suggested that the collapse was due to volcanic activity and concomittant solution of salt in the underlying red beds; however, to date no bedded salts have been found by wells piercing the red beds (Mr. Roy Foster, personal communication). Water of the lake is derived from salt water springs, rain, and snow. Partial water analyses by the Quality of Water Branch of the Ground Water Division of the U. S. Geological Survey are given in Table V.

Field investigation

Several rock samples were collected from the margins of Zuni Salt Lake and the pond inside the crater of the cinder cone. These rocks are basalt cinder blocks and samples of salt saturated soil formed on the basalt at the margins of the pond. No fibers were observed immediately after the rocks were collected, but after they had become thoroughly dried at room temperature in the laboratory, a few salt fibers were observed growing out of vesicles on broken basalt surfaces. The fibers are about 0.03 mm in diameter and from 0.7 to 1.5 mm long. Reflection of light from the sides of the fibers indicate that they have plane sides and probably a square or rectangular cross-section. The thickness of some of the fibers appears to diminish from the base to the apex. A stepped

TABLE V. WATER ANALYSES FROM ZUNI SALT LAKE

Date	2/54 Pond	3/34 Lake	3/34 Pond
Br		35 ppm	10 ppm
Ca		345	280
Mg		2,551	1,117
Na	31,400 ppm	74,976	36,082
K		498	229
HCO_3		235	246
CO_3	502	46	36
SO_4	6,750	14,649	7,546
Cl	46,200	113,149	54,482

An analysis of the harvested salt was obtained by Mr. Foster and is:

K_2SO_4	5.59
$MgCl_2$	1.21
KCl	4.26
NaCl	88.63
	99.69

edge was observed on one fiber, but it could not be determined whether this was due to cleavage or to two adjacent fibers. The fibers are detached quite easily from the substrate, and in all cases they bend rather than break when touched. The fibers are clear and possess high surface perfection under a magnification of X 36. Unfortunately, the fibers were too delicate and too few to be successfully collected for more detailed examination. The existence of crystal faces bounding the fibers and the flexibility of the fibers fits well the description of fibers grown by Gyulai (1954) (see page 10). They seem to be similar to the first type of fiber described in Section IV. Gyulai postulated that growth took place at the apex of the fibers due to a vertical concentration gradient in the atmosphere within the vessel in which growth took place. The fibers observed on the basalt from Zuni Salt Lake, however, could have grown only in a free air environment, and there seems to be no reason to suspect that they grew any differently than fibers grown experimentally during this investigation.

The field area was visited in June, August, and September, and by the last visit, the water level in both the lake and the pond had increased between two and three feet. During the August visit no salt was being precipitated on the floor of the lake because of dilution by rain water, but a salt ledge or bank about 10 inches thick was present at the margin of the pond. This ledge was a mixture of basalt soil and salt. The mixture contained scoria fragments from

pebble to cobble size. The natural fibers described above grew on scoria collected from this zone. It was found that one could dig a foot or more into the ledge without encountering bedrock.

When the area was visited in September, the salt ledge was submerged almost two feet and at the new margin of the pond only a few inches of soil existed above bedrock. Sparse crystalline salt was found at a maximum of about seven feet above the northern margin of the pond during this visit, and at the south side it was found at a maximum of about three feet above the margin of the pond. As the soil at these places was damp, the salt was probably deposited there due to capillary rise and evaporation. The damp soil has a salty taste here.

The author suspects that at the low level of the pond a "soil" or disintegration zone extends through the cone to the Zuni Salt Lake on the north side.

Within the disintegration zone at the surface of the pond, salt impregnated cobble size scoria can be broken with the hands, whereas a hammer is necessary to break the unimpregnated fragments. The weakened condition of some of the salt impregnated scoria and the extensively disintegrated zone at the low level surface of the pond leads one to suspect that the crystallization of salt has had some influence on the disintegration of the rocks here.

The author was not able to find a value for the tensile strength of basalt in the literature, but the International Critical Tables gives a range of 10-30 Kg/cm^2 for sand stone (building stone) and 30-50 Kg/cm^2 for granite (building stone). The tensile strength of a basalt scoria probably lies between that of sandstone and granite and the growth pressure of halite is of this order of magnitude. Therefore, it does not seem improbable that halite could extend fractures in basalt scoria if it crystallized there. Under such near surface conditions as obtained at Zuni Salt Lake, the crystallization of halite must contribute substantially to rock disintegration.

CONCLUSIONS

The maximum growth pressure of NaCl fibers was measured directly, determined graphically, and computed indirectly. The three methods were found to be in substantial agreement. The growth rate was found to vary linearly with the logarithm of the applied pressure. An equation was derived which expressed the maximum growth pressure in terms of growth rate of a crystal and the stress applied to it.

The fibers were found by X-ray analysis to have a [100] orientation and the density of the fiber packing was found to improve with the application of a load. These characteristics of fibrous NaCl are consistent with the theory of preferred orientation set forth by Kamb.

The growth pressure of fibrous NaCl is of geologic significance in that it is of the same order of magnitude as the tensile strengths of sandstone and granite. Geologic evidence gained from examination of rocks at Zuni Salt Lake in New Mexico indicates that under surface conditions, crystallization of halite in fractures can be important in the disintegration of rocks at the margins of salt lakes.

BIBLIOGRAPHY

Amelynkx, S. (1958) The growth of alcalihalide whiskers from solution. Physica, v. 24, pp. 390-392.

Azaroff, L. V. and Buerger, M. J. (1958) The powder method in X-ray crystallography. McGraw-Hill Book Co., N. Y.

Becker, G. F. and Day, A. L. (1905) Proc. Wash. Acad. Sci., v. 7, pp. 283-288 (cited by Buckley, 1951).

--------- and ---------- (1916) Linear force of growing crystals. J. Geol., v. 24, pp. 313-333.

Buckley, H. E. (1951) Crystal growth. John Wiley & Sons, Inc. N. Y.

Bunn, C. W. and Emmett, H. (1949) Crystal growth from solution, Disc. Farad. Soc. no. 5, pp. 119-132.

Chrétien, A., Heubel, J., and Trimolé, P. (1954) Sur la vitesse de cristallization. Comt. Rend. Acad. Sci., v. 239, pp. 814-816.

Cooke, H. C. (1936) Asbestos deposits of the Thetford District, Quebec. Econ. Geol., v. 31, pp. 355-376.

Correns, C. W. (1926) Sitzber. preuss. Akad. Wiss. math.-physik. Klasse, 1926, v. 11, pp. 81-88 (cited by Buckley, 1951).

---------- (1949) Growth and dissolution of crystals under linear pressure. Disc. Farad. Soc., no. 5, pp. 267-271.

Darton, N. H. (1905) The Zuni salt lake. J. Geol., v. 13, pp. 185-193.

Gyulai, Z. (1954) Festigheits und Plastizitatseigenschaften von NaCl-Nadelkristallen. Zeit. fur Phys., v. 138, pp. 317-321.

Herring, C. (1952) The use of classical macroscopic concepts in surface energy problems. Structure and Properties of Solid Surfaces. ed. by R. Gomer and C. S. Smith. pp. 5-72.

Hinegardner, W. S. (1933) Needle shaped crystals of sodium chloride. J. Am. Chem. Soc., v. 55, pp. 1461-1462.

International Critical Tables (1927) v. 2 p. 49.

Kamb, B. W. (1959) Theory of preferred crystal orientation developed by crystallization under stress. Am. J. Sci., v. 67, pp. 153-170.

Kern, R. (1953) Etude du faciès de quelque cristaux ioniques a structure simple. Premiere partie (A). Les changements de faciès en milieu pur. Bull. Soc. franc. Miner. Crist., v. 76, pp. 325-361.

Kossel, W. (1928) in Falkenhagen Quantentheory un Chemie, Liepzig 46 pp. (cited by Buckley, 1951).

Palache, C., Berman, H., and Frondel, C. (1944) The system of mineralogy. v. I pp. 32-33. John Wiley & Sons, N. Y.

Ramberg, H. (1947) The force of crystallization as a well defined property of crystals. Geol. Foren. Forh., v. 69, pp. 189-194.

---------- (1952) The origin of the metamorphic and metasomatic rocks. The Univ. of Chicago Press.

Seidell, A. (1940) Solubilities of inorganic and metal organic compounds. v. 1, p. 1218, D. Van Nostrand Co., N. Y.

Schmidt, R. (1914) Z. Gewinn. Verarb. u. Verwert der Kalisalze v. 8, 21 pp. (cited by Buckley, 1951).

Schubnikov, A. (1934) Z. Krist., v. A88, pp. 466-569 (cited by Buckley, 1951).

Taber, S. (1916a) The growth of crystals under external pressure. Am. J. Sci., v. 41, pp. 532-556.

---------- (1916b) The genesis of asbestos and asbestosform minerals. Bull. A.I.M.E., no. 119, pp. 1973-1998.

Tauber, H. and Kleiner, I. (1932) Needle shaped crystals of sodium chloride obtained by precrystallization. J. Am. Chem. Soc., v. 54, pp. 2392-2393.

Willard, M. E. and Weber, R. H. (1958) Reconnaissance geologic map of Canon Largo thirty-minute quadrangle, N. Mex. Bureau of Mines and Mineral Resources.

Wuerker, R. G. (1956) Annotated tables of strength and elastic properties of rocks, Univ. of Ill. Bull. 663-G.

This thesis is accepted on behalf of the graduate faculty of the Institute by the following committee:

Date: June 3, 1960